

# The NLO twist-3 contribution to the pion electromagnetic form factors in $k_T$ factorization

Shan Cheng, Ying-Ying Fan, and Zhen-Jun Xiao\*

*Department of Physics and Institute of Theoretical Physics,  
Nanjing Normal University, Nanjing, Jiangsu 210023, People's Republic of China,*

(Dated: June 6, 2018)

In this paper, by employing the  $k_T$  factorization theorem, we calculate firstly the next-to-leading-order (NLO) twist-3 contributions to the pion electromagnetic form factors in the  $\pi\gamma^* \rightarrow \pi$  process. From the analytical and numerical calculations we find the following points: (a) For the leading order (LO) twist-2, twist-3 and the NLO twist-2 contributions, our results agree very well with those obtained in previous works; (b) We extract out two factors  $F_{T3}^{(1)}(x_i, t, Q^2)$  and  $\overline{F}_{T3}^{(1)}(x_i, t, Q^2)$ , which describe directly the NLO twist-3 contributions to the pion electromagnetic form factors  $F^+(Q^2)$ ; (c) The NLO twist-3 contribution is negative in sign and cancel partially with the NLO twist-2 part, the total NLO contribution can therefore provide a roughly  $\pm 20\%$  corrections to the total LO contribution in the considered ranges of  $Q^2$ ; and (d) The theoretical predictions for  $Q^2 F^+(Q^2)$  in the low- $Q^2$  region agree well with currently available data, this agreement can be improved by the inclusion of the NLO contributions.

PACS numbers: 12.38.Bx, 12.38.Cy, 12.39.St, 13.20.He

## I. INTRODUCTION

The perturbative QCD (pQCD) factorization approach, based on the  $k_T$  factorization theorem[1–3], have been wildly used to deal with the inclusive and exclusive processes [4–7]. In the  $k_T$  factorization theorem, the end-point singularities are removed by the small but non-zero transverse momentum  $k_T$  of the parton propagators. For many years, the application of the  $k_T$  factorization theorem were mainly at the leading order (LO) level. But the situation changed a lot recently. In Refs. [8–10], the authors calculated the next-to-leading order (NLO) twist-2 contributions to the  $\pi$  transition form factor,  $\pi$  electromagnetic form factor and  $B \rightarrow \pi$  form factor respectively, obtained the infrared finite  $k_T$  dependent NLO hard kernel, and therefore confirmed the applicability of the  $k_T$  factorization to these exclusive processes at the NLO and the leading twist (twist-2) level. This fact tell us that the  $k_T$  factorization approach can also be applied to the high order contributions as mentioned in Ref. [11].

In the framework of the pQCD factorization approach, the contributions to the form factors include four parts:

- (i) The leading order contribution include the leading order twist-2 (LO-T2) contribution and the leading order twist-3 (LO-T3) contribution.
- (ii) The NLO contribution contains the NLO twist-2 (NLO-T2) contribution and the NLO twist-3 (NLO-T3) contribution.

---

\* xiaozhenjun@njnu.edu.cn

At present, the first three parts, namely the LO-T2, LO-T3 and NLO-T2 contributions, have been evaluated in Refs. [8–10], but the NLO-T3 contribution is still absent now.

At leading order level, the LO-T2 part is smaller than the LO-T3 part, by a ratio of  $\sim 34\%$  against  $\sim 66\%$  as shown in Refs. [9, 12, 13]. The NLO-T2 part is around  $20 - 30\%$  of the total leading order contribution (i.e. LO-T2 plus LO-T3 part) in the low  $Q^2$  region. Since the LO-T3 contribution is large, the remaining unknown fourth part, the NLO twist-3 contribution, maybe rather important, and should be calculated in order to obtain the pQCD predictions for relevant form factors at the full NLO level, and to demonstrate that the  $k_T$  factorization theorem is an systematical tool.

In this paper we concentrate on the calculation for the NLO twist-3 contribution to the  $\pi$  electromagnetic form factor, which corresponds to the scattering process  $\pi\gamma^* \rightarrow \pi$ . Our work represents the first calculation for the NLO twist-3 contribution to this quantity in the  $k_T$  factorization theorem.

We know that the collinear divergences would appear when the massless gluon is emitted from the light external line as the gluon is paralleled to the initial- or the final-state pion which are massless assumed. The soft divergences would come from the exchange of the massless gluon between two on-shell external lines. In this work light partons are considered to be off-shell by  $k_T^2$  to regulated the infrared divergences in both the QCD quark diagrams and the effective diagrams for pion wave functions. It's a nontrivial work to verify that the collinear divergences from the quark-level diagrams offset those from the pion wave functions and the soft divergences cancel among quark-level diagrams exactly at the twist-3 level as well as at the leading twist-2 case [9]. As demonstrated in Refs. [9, 10], both the large double logarithms  $\alpha_s \ln^2(k_T)$  and  $\alpha_s \ln^2(x_i)$ , here  $x_i$  being the parton momentum fraction of the anti-quark in the meson wave functions, could be absorbed through the resummation technology. The double logarithm  $\alpha_s \ln^2(k_T)$  would be absorbed into the  $\pi$  meson wave functions and then been summed to all orders in the coupling constant  $\alpha_s$  by the  $k_T$  resummation[3]. The jet function would included when there exist the end-point singularity in the hard kernel, and then the double logarithm  $\alpha_s \ln^2(x_i)$  would be summed to all orders by the threshold resummation[14, 15]. The renormalization scale  $\mu$  and the factorization scale  $\mu_f$  are introduced in the high-order corrections to the QCD quark diagrams and the effective diagrams, respectively. With the appropriate choice of the scale  $\mu$  and  $\mu_f$ , say setting them as the internal hard scale as postulated in [9], the NLO correction are under control.

This paper is organized as follows. In section. II, we give a brief review about the evaluations of the LO diagrams for the process  $\pi\gamma^* \rightarrow \pi$ , for both the twist-2 part and twist-3 part. In section. III,  $O(\alpha_s^2)$  QCD quark diagrams for the process will be calculated with the inclusion of the twist-3 contributions. The convolutions of  $O(\alpha_s)$  (NLO) effective diagrams for the meson wave functions and  $O(\alpha_s)$  (LO) hard kernel would also be presented in this section, then the  $k_T$ -dependent NLO hard kernel at twist-3 will be obtained. Section. IV contains the numerical analysis. With appropriate choices for the renormalization scale  $\mu$ , the factorization scale  $\mu_f$  and the input meson wave functions, we make the numerical calculations for all four parts of the LO and NLO contributions to the pion electromagnetic form factor in the  $\pi\gamma^* \rightarrow \pi$  process. Section V contains the conclusions.

## II. LO TWIST-2 AND TWIST-3 CONTRIBUTIONS

The leading order hard kernels of the  $\pi$  electromagnetic form factor as shown in Fig. 1 are calculated in this section. The  $\pi\gamma^* \rightarrow \pi$  form factors are defined via the matrix element

$$\begin{aligned} \langle \pi(p_2) | J^\mu | \pi(p_1) \rangle &= f_1(q^2) p_1^\mu + f_2(q^2) p_2^\mu \\ &= F^+(q^2) (p_1^\mu + p_2^\mu), \end{aligned} \quad (1)$$

where  $p_1$  ( $p_2$ ) refers to the momentum of the initial (final) state pion,  $q = p_1 - p_2$  is the momentum transferred in the weak vertex. Using the same definitions for the leading case as being used in Ref. [9], the momentum  $p_1$  and  $p_2$  are chosen as

$$p_1 = (p_1^+, 0, \mathbf{0}_T), \quad p_2 = (0, p_2^-, \mathbf{0}_T), \quad (2)$$

with  $q^2 = -2p_1 \cdot p_2 = -Q^2$ . According to the  $k_T$  factorization, the  $k_1 = (x_1 p_1^+, 0, k_{1T})$  in the initial pion meson and  $k_2 = (0, x_2 p_2^-, k_{2T})$  in the final pion meson as labeled in Fig. 1, and  $x_1$  and  $x_2$  being the momentum fractions. The follow hierarchy is postulated in the small- $x$  region:

$$Q^2 \gg x_2 Q^2 \sim x_1 Q^2 \gg x_1 x_2 Q^2 \gg k_{1T}^2, k_{2T}^2, \quad (3)$$

The following Fierz identity is employed to factorize the fermion flow.

$$\begin{aligned} I_{ij} I_{lk} &= \frac{1}{4} I_{ik} I_{lj} + \frac{1}{4} (\gamma_5)_{ik} (\gamma_5)_{lj} + \frac{1}{4} (\gamma^\alpha)_{ik} (\gamma^\alpha)_{lj} \\ &\quad + \frac{1}{4} (\gamma_5 \gamma^\alpha)_{ik} (\gamma_\alpha \gamma_5)_{lj} + \frac{1}{8} (\sigma^{\alpha\beta} \gamma_5)_{ik} (\sigma_{\alpha\beta} \gamma_5)_{lj}. \end{aligned} \quad (4)$$

The identity matrix  $I$  here is a 4 dimension matrix, the structure  $\gamma_\alpha \gamma_5$  in Eq. (4) contribute at the leading twist (twist-2), while  $\gamma_5$  and  $\sigma_{\alpha\beta} \gamma_5$  contribute at twist-3 level. The identity of  $SU(3)_c$  group,

$$I_{ij} I_{lk} = \frac{1}{N_c} I_{lj} I_{ik} + 2(T^c)_{lj} (T^c)_{ik} \quad (5)$$

is also employed to factorize the color flow. In Eq. (5),  $(i, j, l, k)$  are color index,  $N_c = 3$  is the number of the colors, and  $T^c$  is the Gel-Mann color matrix of  $SU(3)_c$ . The first term in Eq. (5) corresponds to the color-singlet state of the valence quark and the anti-quark, while the second term will be associated with the color-octet state.

We here consider only the subdiagram Fig. 1(a) in detail, where the quark and anti-quark form a color-singlet state. The hard kernels of the other subdiagrams can be obtained by simply kinetic replacements. The wave function  $\Phi_\pi(p_i, x_i)$  for the initial and final state pion can be written as the following form [17–19]

$$\Phi_\pi(p_1, x_1) = \frac{i}{\sqrt{2N_c}} \gamma_5 \{ \not{p}_1 \phi_\pi^A(x_1) + m_0 [\phi_\pi^P(x_1) - (\not{n}_+ \not{n}_- - 1) \phi_\pi^T(x_1)] \}, \quad (6)$$

$$\Phi_\pi(p_2, x_2) = \frac{i}{\sqrt{2N_c}} \gamma_5 \{ \not{p}_2 \phi_\pi^A(x_2) + m_0 [\phi_\pi^P(x_2) - (\not{n}_- \not{n}_+ - 1) \phi_\pi^T(x_2)] \}, \quad (7)$$

where  $n_+ = (1, 0, \mathbf{0}_T)$  and  $n_- = (0, 1, \mathbf{0}_T)$  denote the unit vector along with the positive and negative  $z$ -axis direction,  $m_0 = 1.74$  GeV is the chiral mass of pion,  $N_c$  is the number of colors,  $\phi_\pi^A(x_i)$  are the leading twist-2 pion distribution amplitude, while  $\phi_\pi^P(x_i)$  and  $\phi_\pi^T(x_i)$  are the twist-3 pion distribution amplitudes.

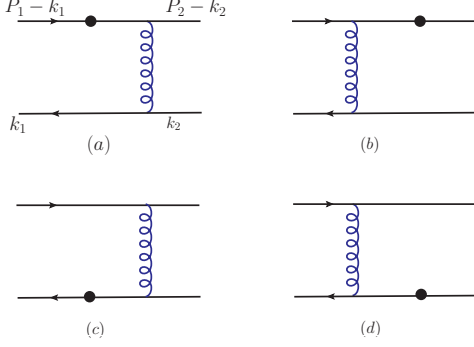


FIG. 1. Leading-order quark diagrams for the  $\pi\gamma^* \rightarrow \pi$  form factor with  $\bullet$  representing the virtual photon vertex.

Combining the decompositions in Eq. (4) and Eq. (5), we then can sandwich Fig. 1(a) with the structures

$$\frac{1}{4N_c} \not{p}_1 \gamma_5, \quad \frac{1}{4N_c} \gamma_5 \not{p}_2, \quad (8)$$

from the initial and final state respectively, in order to obtain the hard kernel  $H^{(0)}$  at twist-2 level. For the derivation of the twist-3 hard kernel, one should sandwich Fig. 1(a) with the following two sets of structures

$$\left( \frac{1}{4N_c} \gamma_5, \quad \frac{1}{4N_c} \gamma_5 \right); \quad \left( \frac{1}{8N_c} \sigma^{\alpha\beta} \gamma_5, \quad \frac{1}{8N_c} \sigma_{\alpha\beta} \gamma_5 \right). \quad (9)$$

Then the LO twist-3 contribution to the hard kernel from Fig. 1(a) can be written as[20]

$$H_a^{(0)}(x_1, k_{1T}, x_2, k_{2T}) = (-2ie_q)4\pi\alpha_s \frac{C_F}{16N_c} m_0^2 \phi_\pi^P(x_2) \cdot \left\{ \frac{-4p_2^\mu [\phi_\pi^P(x_1) - \phi_\pi^T(x_1)]}{(p_2 - k_1)^2 (k_1 - k_2)^2} + \frac{4x_1 p_1^\mu [\phi_\pi^P(x_1) + \phi_\pi^T(x_1)]}{(p_2 - k_1)^2 (k_1 - k_2)^2} \right\}, \quad (10)$$

where  $\alpha_s$  is the strong coupling constant,  $C_F = 4/3$  is color factor,  $e_q$  refers to the charge of the quark interacting with the  $\gamma^*$  in  $\pi\gamma^* \rightarrow \pi$  process.

The corresponding LO twist-2 contribution to the hard kernel takes the form of

$$H_{a,T2}^{(0)}(x_1, k_{1T}, x_2, k_{2T}) = (ie_q)4\pi\alpha_s \frac{C_F}{16N_c} Q^2 \phi_\pi^A(x_2) \phi_\pi^A(x_1) \cdot \frac{4x_1 p_1^\mu}{(p_1 - k_2)^2 (k_1 - k_2)^2}, \quad (11)$$

It is easy to see that all parts of the initial state pion, the twist-2  $\phi_\pi^A(x_1)$  and twist-3  $\phi_\pi^P(x_1)$  and  $\phi_\pi^T(x_1)$ , provide contributions at leading order level, but only the  $\phi_\pi^A(x_2)$  and  $\phi_\pi^P(x_2)$  of the final state pion contribute at LO level, because the contribution from the  $\phi_\pi^T(x_2)$  component become zero when it is contracting with the gluon propagator. For the LO twist-3 hard kernel  $H_a^{(0)}(x_1, k_{1T}, x_2, k_{2T})$ , one can see that it contains two lorentz structures:  $p_2^\mu$  term and  $x_1 p_1^\mu$  term, these two terms all should be included in the numerical calculations. For the LO twist-2 hard kernel  $H_{a,T2}^{(0)}$  as given in Eq. (11), it depends on one term  $x_1 p_1^\mu$  only. From previous studies in Ref.[9, 12, 13], we know that the LO twist-2 part is only about half of the LO twist-3 part. So one generally expect that the NLO twist-3 contribution maybe large and essential for considered transitions, which is also one of the motivations of this paper.

### III. NLO CORRECTIONS

Under the hierarchy as shown in Eq. (3), only those terms which don't vanish in the limits of  $x \rightarrow 0$  and  $k_{iT} \rightarrow 0$  should be kept, this fact does simplify the expressions of the NLO contributions greatly.

From the discussions at the end of Sec. I, we know that both lorentz structures  $x_1 p_1^\mu$  and  $p_2^\mu$  will contribute. From the hard kernel  $H_a^{(0)}(x_1, k_{1T}, x_2, k_{2T})$  as given in Eq. (10), we define those two parts of the LO twist-3 contribution,  $H_a^{(0)}(x_1 p_1^\mu)$  and  $H_a^{(0)}(p_2^\mu)$  in the form of

$$H_a^{(0)}(x_1 p_1^\mu) \equiv (-2ie_q)4\pi\alpha_s \frac{C_F}{16N_c} m_0^2 \phi_\pi^P(x_2) \frac{4x_1 p_1^\mu [\phi_\pi^P(x_1) - \phi_\pi^T(x_1)]}{(p_2 - k_1)^2 (k_1 - k_2)^2}, \quad (12)$$

$$H_a^{(0)}(p_2^\mu) \equiv (-2ie_q)4\pi\alpha_s \frac{C_F}{16N_c} m_0^2 \phi_\pi^P(x_2) \frac{-4p_2^\mu [\phi_\pi^P(x_1) + \phi_\pi^T(x_1)]}{(p_2 - k_1)^2 (k_1 - k_2)^2}, \quad (13)$$

$$H_a^{(0)} = H_a^{(0)}(x_1 p_1^\mu) + H_a^{(0)}(p_2^\mu). \quad (14)$$

For Figs. 1(b,c,d), one can find the corresponding LO twist-3 contributions by simple replacements. For the sake of simplicity, we will generally omit the subscript “a” in  $H_a^{(0)}$  in the following sections, unless stated specifically.

#### A. NLO twist-3 Contributions of the QCD Quark Diagrams

Now we calculate the NLO twist-3 contributions to Fig. 1(a), which comes from the self-energy diagrams, the vertex diagrams, the box and the pentagon diagrams, as illustrated in Figs. 2,3 and 4 respectively. After completing the calculations for Fig. 1(a), we can obtain the results for other three figures: Fig. 1(b,c,d), by simple replacements.

The ultraviolet(UV) divergences are extracted in the dimensional reduction [21] in order to avoid the ambiguity from handing the matrix  $\gamma_5$ . The infrared(IR) divergences are identified as the logarithms  $\ln \delta_1$ ,  $\ln \delta_2$  and their combinations, as defined in Ref. [9]

$$\delta_1 = \frac{k_{1T}^2}{Q^2}, \quad \delta_2 = \frac{k_{2T}^2}{Q^2}, \quad \delta_{12} = \frac{-(k_1 - k_2)^2}{Q^2}. \quad (15)$$

The self-energy corrections obtained by evaluating the one-loop Feynman diagrams in Fig. 2(a-f) are of the form

$$G_{2a}^{(1)} = -\frac{\alpha_s C_F}{8\pi} \left[ \frac{1}{\epsilon} + \ln \frac{4\pi\mu^2}{\delta_1 Q^2 e^{\gamma_E}} + 2 \right] H^{(0)},$$

$$G_{2b}^{(1)} = -\frac{\alpha_s C_F}{8\pi} \left[ \frac{1}{\epsilon} + \ln \frac{4\pi\mu^2}{\delta_1 Q^2 e^{\gamma_E}} + 2 \right] H^{(0)}, \quad (16)$$

$$G_{2c}^{(1)} = -\frac{\alpha_s C_F}{8\pi} \left[ \frac{1}{\epsilon} + \ln \frac{4\pi\mu^2}{\delta_2 Q^2 e^{\gamma_E}} + 2 \right] H^{(0)},$$

$$G_{2d}^{(1)} = -\frac{\alpha_s C_F}{8\pi} \left[ \frac{1}{\epsilon} + \ln \frac{4\pi\mu^2}{\delta_2 Q^2 e^{\gamma_E}} + 2 \right] H^{(0)},$$

$$G_{2e}^{(1)} = -\frac{\alpha_s C_F}{4\pi} \left[ \frac{1}{\epsilon} + \ln \frac{4\pi\mu^2}{x_1 Q^2 e^{\gamma_E}} + 2 \right] H^{(0)},$$

$$G_{2f+2g+2h+2i}^{(1)} = \frac{\alpha_s}{4\pi} \left[ \left( \frac{5}{3} N_c - \frac{2}{3} N_f \right) \left( \frac{1}{\epsilon} + \ln \frac{4\pi\mu^2}{\delta_{12} Q^2 e^{\gamma_E}} \right) \right] H^{(0)}, \quad (17)$$

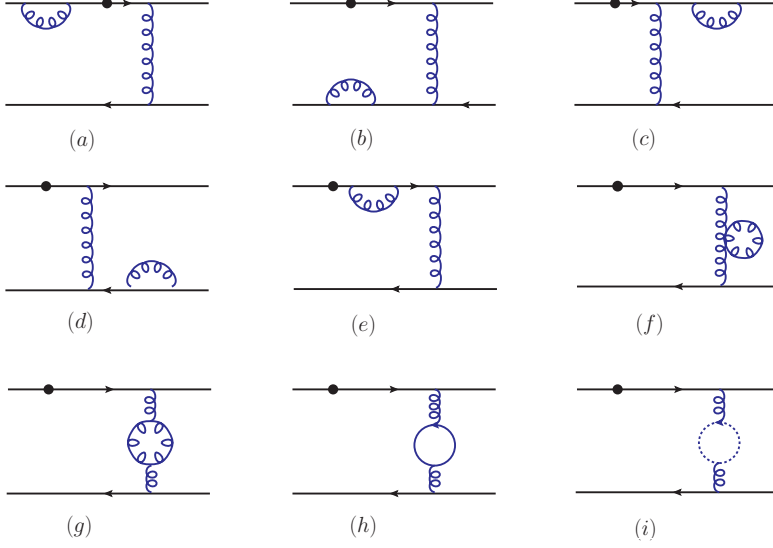


FIG. 2. Self-energy corrections to Fig.1(a).

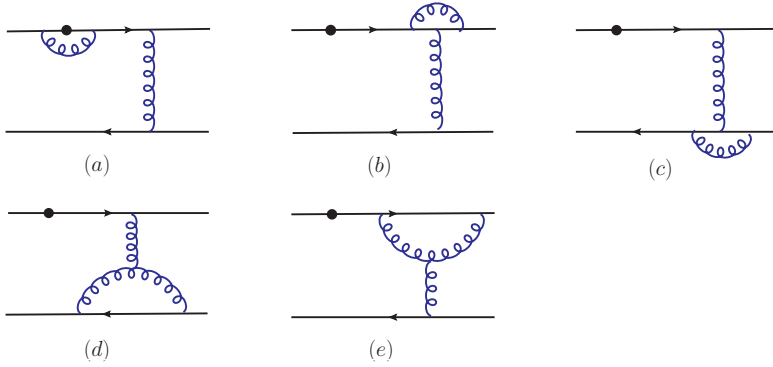


FIG. 3. Vertex corrections to Fig.1(a).

where  $1/\epsilon$  represents the UV pole term,  $\mu$  is the renormalization scale,  $\gamma_E$  is the Euler constant,  $N_c$  is the number of quark color,  $N_f$  is the number of the active quarks flavors, and  $H^{(0)}$  denotes the LO twist-3 hard kernel described in Eq. (10). The Fig. 2(f,g,h,i) denotes the self-energy correction to the exchanged gluon.

It is easy to find that, the NLO self-energy corrections to the LO twist-3 hard kernels as listed in Eq. (17) are identical in form to those self-energy corrections to the LO twist-2 hard kernels as given in Eqs. (6-9) in Ref. [9]. The reason is that the self-energy diagrams don't involve the external lines and therefore are irrelevant with the twist structures of the wave functions. It should be note that an additional symmetry factor  $\frac{1}{2}$  appeared from the choice of the gluon endpoint to attach the external line in the self-energy correction Fig. 2(a,b,c,d). The self-energy corrections to the external lines will be canceled by the responding effective diagrams as shown in Fig. (5,6). The self-energy correction to the internal quark line as shown in Fig. 2(e) don't generate any IR

divergences.

The vertex corrections obtained by evaluating the one-loop Feynman diagrams in Fig. 3(a-e) are of the form

$$\begin{aligned}
G_{3a}^{(1)} &= \frac{\alpha_s C_F}{4\pi} \left[ \frac{1}{\epsilon} + \ln \frac{4\pi\mu^2}{Q^2 e^{\gamma_E}} + \frac{1}{2} \right] H^{(0)}, \\
G_{3b}^{(1)} &= -\frac{\alpha_s}{8\pi N_c} \left[ \frac{1}{\epsilon} + \ln \frac{4\pi\mu^2}{x_1 Q^2 e^{\gamma_E}} - 1 \right] H^{(0)} \\
&\quad - \frac{\alpha_s}{8\pi N_c} \left[ 1 - \ln \frac{\delta_2}{x_1} \right] H^{(0)}(x_1 p_1^\mu), \\
G_{3c}^{(1)} &= -\frac{\alpha_s}{8\pi N_c} \left[ \frac{1}{\epsilon} + \ln \frac{4\pi\mu^2}{\delta_{12} Q^2 e^{\gamma_E}} \right] H^{(0)} \\
&\quad - \frac{\alpha_s}{8\pi N_c} \left[ \ln \frac{\delta_2}{\delta_{12}} \ln \frac{\delta_1}{\delta_{12}} + \ln \frac{\delta_1}{\delta_{12}} + \ln \frac{\delta_2}{\delta_{12}} + \frac{\pi^2}{3} \right] H^{(0)}(p_2^\mu), \\
G_{3d}^{(1)} &= \frac{\alpha_s N_c}{8\pi} \left[ \frac{3}{\epsilon} + 3 \ln \frac{4\pi\mu^2}{\delta_{12} Q^2 e^{\gamma_E}} + \frac{11}{2} \right] H^{(0)} \\
&\quad - \frac{\alpha_s N_c}{8\pi} \left[ \ln \frac{\delta_1}{\delta_{12}} + \ln \frac{\delta_2}{\delta_{12}} \right] H^{(0)}(p_2^\mu) \\
G_{3e}^{(1)} &= \frac{\alpha_s N_c}{8\pi} \left[ \frac{3}{\epsilon} + 3 \ln \frac{4\pi\mu^2}{x_1 Q^2 e^{\gamma_E}} + \frac{11}{2} \right] H^{(0)} \\
&\quad - \frac{\alpha_s N_c}{8\pi} \left[ \ln \frac{\delta_2}{x_1} \ln x_2 + \ln \frac{\delta_2}{x_1} \right] H^{(0)}(x_1 p_1^\mu). \tag{18}
\end{aligned}$$

It is easy to find that the NLO twist-3 corrections to the LO hard kernel  $H^{(0)}$  in Eq. (14) have the UV divergence and they have the same divergence behavior in the self-energy and the vertex corrections. The summation of these UV divergences leads to the same result as the one for the NLO twist-2 case [9]

$$\frac{\alpha_s}{4\pi} \left( 11 - \frac{2}{3} N_f \right) \frac{1}{\epsilon}, \tag{19}$$

which meets the requirement of the universality of the wave functions.

The amplitude  $G_{3a}^{(1)}$  have no IR divergence due to the fact that the numerator in the amplitude of the collinear region is dominated by the transverse contributions which are negligible in Fig. 3(a). IR divergences in  $G_{3c}^{(1)}$  and  $G_{3d}^{(1)}$  are only relevant with the hard kernel  $H^{(0)}(p_2^\mu)$ , which is induced by the singular gluon attaches to the down quark lines. Similarly, IR divergences in  $G_{3b}^{(1)}$  and  $G_{3e}^{(1)}$  only occur in the hard kernel  $H^{(0)}(x_1 p_1^\mu)$  since the singular gluon is attached to the up quark lines.

The amplitude  $G_{3b}^{(1)}$  should have collinear divergence because the radiative gluon in Fig. 3(b) is attached to the light valence quark of the final state pion, and we find that the IR contribution is regulated by  $\ln \delta_2$ . Both the collinear and soft divergences are produced in  $G_{3c}^{(1)}$  because the radiative gluon in Fig. 3(c) is attached to the external light valence anti-quarks. The large double logarithm  $\ln \delta_1 \ln \delta_2$  comes from the overlap of the IR divergences, and will be canceled by the large double logarithm term from Fig. 4(f).

The radiative gluon in Fig. 3(d) is attached to the light valence anti-quarks as well as the virtual LO hard gluon, so the soft divergence and the large double logarithm aren't generated in  $G_{3d}^{(1)}$ . The



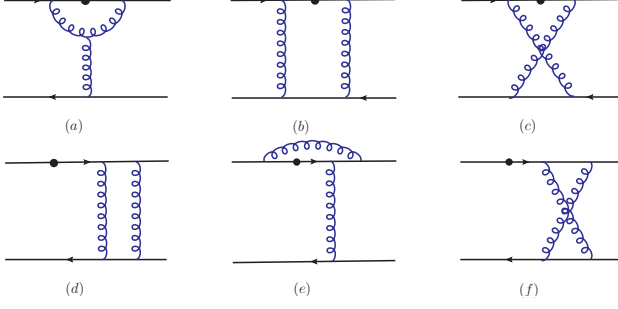


FIG. 4. Box and pentagon corrections to Fig.1(a).

radiative gluon in Fig. 3(e) is attached only to the light valence quark as well as the virtual LO hard gluon, and then  $G_{3e}^{(1)}$  just contains the collinear divergence regulated by  $\ln \delta_2$  in the  $l \parallel P_2$  region.

The NLO twist-3 contributions from the box and pentagon diagrams as shown in Fig. 4 are summarized as

$$\begin{aligned}
 G_{4a}^{(1)} &= -\frac{\alpha_s N_c}{8\pi} \left[ (1 + \ln x_1) \ln \delta_1 - (1 + \frac{3}{2} \ln x_1) \ln x_2 + \frac{1}{8} + \frac{\pi^2}{12} \right] H^{(0)}(x_1 p_1^\mu), \\
 &\quad -\frac{\alpha_s N_c}{8\pi} \left[ (1 + \ln x_2) \ln \delta_2 - (1 + \frac{3}{2} \ln x_2) \ln x_1 + \frac{1}{8} + \frac{\pi^2}{12} \right] H^{(0)}(x_2 p_2^\mu), \\
 G_{4b}^{(1)} &\equiv 0, \\
 G_{4c}^{(1)} &= -\frac{\alpha_s}{8\pi N_c} \left[ \ln \frac{x_1}{\delta_2} \ln \frac{x_2}{\delta_1} + \ln^2 x_2 \right] H^{(0)}(x_1 p_1^\mu) \\
 &\quad -\frac{\alpha_s}{8\pi N_c} \left[ \ln \frac{x_2}{\delta_1} \ln \frac{x_1}{\delta_2} + \ln^2 x_1 \right] H^{(0)}(x_2 p_2^\mu), \\
 G_{4d}^{(1)} &\equiv 0, \\
 G_{4e}^{(1)} &= \frac{\alpha_s}{8\pi N_c} \left[ \ln \delta_1 \ln \delta_2 + \ln \delta_1 + \frac{5}{4} \right] H^{(0)}(x_1 p_1^\mu), \\
 G_{4f}^{(1)} &= -\frac{\alpha_s}{8\pi N_c} \left[ \ln \frac{\delta_1}{\delta_{12}} \ln \frac{\delta_2}{\delta_{12}} - 2 \ln 2 - 1 \right] H^{(0)}(p_2^\mu). \tag{20}
 \end{aligned}$$

Because of the properties of the propagators in above four- and five-point integrals, there is no UV divergences in above amplitudes. Fig. 4(b) and 4(d) are two-particle reducible diagrams, their contribution should be canceled by the corresponding effective diagrams Fig. 5(c) and Fig. 6(c) for the NLO initial and final state meson wave functions due to the requirement of the factorization theorem, so we can set them zero safely.

The  $H^{(0)}(x_2 p_2^\mu)$  terms appeared in  $G_{4a}^{(1)}$  and  $G_{4c}^{(1)}$  are obtained from the evaluation of Fig. 4(a) and 4(c) only. The LO hard kernel  $H^{(0)}(x_2 p_2^\mu)$  has the same form as the  $H^{(0)}(x_1 p_1^\mu)$  as defined in Eq. (12) but with replacements of  $x_1 \rightarrow x_2$  and  $p_1^\mu \rightarrow p_2^\mu$ . IR regulators only appear to the hard kernel  $H^{(0)}(x_1 p_1^\mu)$  of the Fig. 4(a,c,e), which are decided by the fact that the left end-point of the emission gluon is attached to the up light external line. Similarly, Fig. 4(f) only grow the IR regulators to the hard kernel  $H^{(0)}(p_2^\mu)$ . Note that the emission gluon in Fig. 4(c,e,f) is attached to external light lines, so it's amplitude would dominated in the collinear regions and soft region, then the double logarithm would appear. The attaching of the emission gluon in Fig. 4(a) to the



initial external line and the LO hard kernel deduce that only IR regulator  $\ln \delta_1$  is grown in the amplitude  $G_{4a}^{(1)}$ .

Now we just consider the IR parts regulated by  $\ln \delta_i$  which would not be canceled directly by their counterparts from the effective diagrams of Fig. 5. These IR pieces appear in  $G_{3b,3c,3d,3e}^{(1)}$  and  $G_{4a,4c,4e,4f}^{(1)}$ . We class these amplitudes into two sets according to the hard kernels to which those IR regulators  $\ln \delta_i$  give corrections. Then the first set includes  $G_{3c,3d}^{(1)}$  and  $G_{4f}^{(1)}$ , while the second set contains  $G_{3b,3e}^{(1)}$  and  $G_{4a,4c,4e}^{(1)}$  terms. These amplitudes are calculated in the leading IR regions to check the  $k_T$  factorization theorem.

We firstly evaluate the NLO twist-3 corrections to  $H^{(0)}(p_2^\mu)$ . The amplitudes  $G_{3c,3d}^{(1)}$  and  $G_{4f}^{(1)}$  are recalculated by employing the phase space slicing method [16],

$$\begin{aligned} G_{3c}^{(1)}(l \rightarrow 0) &= \frac{\alpha_s}{8\pi N_c} \left[ \ln \frac{\delta_1}{\delta_{12}} \ln \frac{\delta_2}{\delta_{12}} + \frac{\pi^2}{3} \right] H^{(0)}(p_2^\mu), \\ G_{3c}^{(1)}(l \parallel p_1) &= \frac{\alpha_s}{8\pi N_c} \left[ \ln \frac{\delta_1}{\delta_{12}} \ln \frac{\delta_2}{\delta_{12}} + \ln \frac{\delta_1}{\delta_{12}} \right] H^{(0)}(p_2^\mu), \\ G_{3c}^{(1)}(l \parallel p_2) &= \frac{\alpha_s}{8\pi N_c} \left[ \ln \frac{\delta_1}{\delta_{12}} \ln \frac{\delta_2}{\delta_{12}} + \ln \frac{\delta_2}{\delta_{12}} \right] H^{(0)}(p_2^\mu). \end{aligned} \quad (21)$$

$$\begin{aligned} G_{3d}^{(1)}(l \parallel p_1) &= \frac{\alpha_s N_c}{8\pi} \left[ -\ln \frac{\delta_1}{\delta_{12}} \right] H^{(0)}(p_2^\mu), \\ G_{3d}^{(1)}(l \parallel p_2) &= \frac{\alpha_s N_c}{8\pi} \left[ -\ln \frac{\delta_2}{\delta_{12}} \right] H^{(0)}(p_2^\mu). \end{aligned} \quad (22)$$

$$\begin{aligned} G_{4f}^{(1)}(l \rightarrow 0) &= -\frac{\alpha_s}{8\pi N_c} \left[ \ln \frac{\delta_1}{\delta_{12}} \ln \frac{\delta_2}{\delta_{12}} + \frac{\pi^2}{3} \right] H^{(0)}(p_2^\mu), \\ G_{4f}^{(1)}(l \parallel p_1) &= -\frac{\alpha_s}{8\pi N_c} \left[ \ln \frac{\delta_1}{\delta_{12}} \ln \frac{\delta_2}{\delta_{12}} + \frac{\pi^2}{6} - 1 \right] H^{(0)}(p_2^\mu), \\ G_{4f}^{(1)}(l \parallel p_2) &= -\frac{\alpha_s}{8\pi N_c} \left[ \ln \frac{\delta_1}{\delta_{12}} \ln \frac{\delta_2}{\delta_{12}} + \frac{\pi^2}{6} - 2 \ln 2 \right] H^{(0)}(p_2^\mu). \end{aligned} \quad (23)$$

By summing up all terms in Eq. (21,22,23), one finds that the soft contributions in the limit  $l \rightarrow 0$  from Fig. 3(c) and Fig. 4(f) are canceled each other, while the remaining collinear contributions in the regions of  $l \parallel p_1$  and  $l \parallel p_2$  are of the form,

$$G_{3c+3d+4f}^{(1)}(l \parallel p_1) = -\frac{\alpha_s C_F}{8\pi} [2 \ln \delta_1] H^{(0)}(p_2^\mu), \quad (24)$$

$$G_{3c+3d+4f}^{(1)}(l \parallel p_2) = -\frac{\alpha_s C_F}{8\pi} [2 \ln \delta_2] H^{(0)}(p_2^\mu), \quad (25)$$

The IR contributions to NLO twist-3 corrections to  $H^{(0)}(x_1 p_1^\mu)$  can be obtained in similar way.

$$G_{3b}^{(1)}(l \parallel p_2) = -\frac{\alpha_s}{8\pi N_c} \left[ 1 - \ln \frac{\delta_2}{x_1} \right] H^{(0)}(x_1 p_1^\mu), \quad (26)$$

$$G_{3e}^{(1)}(l \parallel p_2) = -\frac{\alpha_s N_c}{8\pi} \left[ \ln \frac{\delta_2}{x_1} (\ln x_2 + 1) \right] H^{(0)}(x_1 p_1^\mu), \quad (27)$$

$$G_{4a}^{(1)}(l \parallel p_1) = -\frac{\alpha_s N_c}{8\pi} \left[ \ln \delta_1 (\ln x_1 + 1) - \ln x_2 \left( \frac{3}{2} \ln x_1 + 1 \right) + \frac{\pi^2}{12} + \frac{1}{8} \right] H^{(0)}(x_1 p_1^\mu), \quad (28)$$

$$\begin{aligned} G_{4c}^{(1)}(l \rightarrow 0) &= -\frac{\alpha_s}{8\pi N_c} \left[ \ln \delta_1 \ln \delta_2 + \frac{\pi^2}{3} \right] H^{(0)}(x_1 p_1^\mu), \\ G_{4c}^{(1)}(l \parallel p_1) &= -\frac{\alpha_s}{8\pi N_c} \left[ \ln \delta_1 \ln \frac{\delta_2}{x_1} + \frac{\pi^2}{6} \right] H^{(0)}(x_1 p_1^\mu), \\ G_{4c}^{(1)}(l \parallel p_2) &= -\frac{\alpha_s}{8\pi N_c} \left[ \ln \delta_2 \ln \frac{\delta_1}{x_2} + \ln x_2 (\ln x_2 + \ln x_1) + \frac{\pi^2}{6} \right] H^{(0)}(x_1 p_1^\mu), \end{aligned} \quad (29)$$

$$\begin{aligned} G_{4e}^{(1)}(l \rightarrow 0) &= \frac{\alpha_s}{8\pi N_c} \left[ \ln \delta_1 \ln \delta_2 + \frac{\pi^2}{3} \right] H^{(0)}(x_1 p_1^\mu), \\ G_{4e}^{(1)}(l \parallel p_1) &= \frac{\alpha_s}{8\pi N_c} \left[ \ln \delta_1 \ln \delta_2 + \ln \delta_1 - \ln x_1 + \frac{\pi^2}{6} + 3 \right] H^{(0)}(x_1 p_1^\mu), \\ G_{4e}^{(1)}(l \parallel p_2) &= \frac{\alpha_s}{8\pi N_c} \left[ \ln \delta_1 \ln \delta_2 + \frac{3}{2} \ln x_1 + \frac{\pi^2}{6} - \frac{7}{4} \right] H^{(0)}(x_1 p_1^\mu). \end{aligned} \quad (30)$$

Again, the soft parts from Fig. 4(c) and Fig. 4(e) are canceled each other, while the remaining collinear contributions to the LO hard kernel  $H^{(0)}(x_1 p_1^\mu)$ , after summing up the amplitudes as given in Eqs. (26,27,28, 29,30), are the following

$$\begin{aligned} G_{4a+4c+4e}^{(1)}(l \parallel p_1) &= -\frac{\alpha_s C_F}{8\pi} [2 \ln \delta_1 (\ln x_1 + 1)] H^{(0)}(x_1 p_1^\mu), \\ G_{3b+3e+4c+4e}^{(1)}(l \parallel p_2) &= -\frac{\alpha_s C_F}{8\pi} [2 \ln \delta_2 (\ln x_2 + 1)] H^{(0)}(x_1 p_1^\mu). \end{aligned} \quad (31)$$

Note that we have dropped the constant terms in Eqs. (25,31) since we here consider the IR parts only. According to previous studies in Refs.[8–10], we know that these IR divergences could be absorbed into the NLO wave functions of the pion mesons. This point will become clear after we complete the calculations for the effective diagrams in Fig. 5 and Fig. 6. This absorption means that the  $k_T$  factorization is valid at the NLO level for the  $\pi \gamma^* \rightarrow \pi$  process.

Without the reducible diagrams  $G_{2a,2b,2c,2d,4b,4d}^{(1)}$ , the summation for the NLO twist-3 contributions from all the irreducible QCD quark diagrams as illustrated by Figs. (2,3,4) leads to the final

result for  $G^{(1)}$ :

$$\begin{aligned}
G^{(1)} = & \frac{\alpha_s C_F}{8\pi} \left[ \frac{29}{2} \left( \frac{1}{\epsilon} + \ln \frac{4\pi\mu^2}{Q^2 e^{\gamma_E}} \right) - 2 \ln \delta_1 (\ln x_1 + 1) - 2 \ln \delta_2 (\ln x_2 + 1) \right. \\
& - \frac{21}{8} \ln(x_1 x_2) - \frac{23}{8} \ln x_1 - \frac{1}{4} \ln^2 x_2 - \frac{9}{4} \ln x_2 - \frac{3\pi^2}{16} + \frac{721}{32} \left. \right] H^{(0)}(x_1 p_1^\mu) \\
& + \frac{\alpha_s C_F}{8\pi} \left[ \frac{29}{2} \left( \frac{1}{\epsilon} + \ln \frac{4\pi\mu^2}{Q^2 e^{\gamma_E}} \right) - 2 \ln \delta_1 - 2 \ln \delta_2 \right. \\
& - 4 \ln(x_1 x_2) - 5 \ln x_1 + \frac{\pi^2}{12} + \frac{\ln 2}{2} + 23 \left. \right] H^{(0)}(p_2^\mu), \tag{32}
\end{aligned}$$

for  $N_f = 6$ . The UV divergence in above expression is the same one as in the pion electromagnetic form factor [9], which determines the renormalization-group(RG) evolution of the strong coupling constant  $\alpha_s$ .

### B. Convolution of the $O(\alpha_s)$ wave functions with the LO hard kernel

A basic argument of  $k_T$  factorization is that the IR divergences from the NLO corrections can also be absorbed into the non-perturbative wave functions which are universal. From this point, the convolution of the NLO wave functions and the LO hard kernel  $H^{(0)}$  are computed, and the resultant IR part should cancel the IR divergences appeared in the NLO amplitude  $G^{(1)}$  as given in Eq. (32).

The convolution of the NLO pion wave functions and the LO hard kernel are calculated in this subsection. In  $k_T$  factorization theorem, the  $\Phi_{\pi,P}^{(1)}$  and  $\Phi_{\pi,T}^{(1)}$  collect the  $O(\alpha_s)$  effective diagrams for the twist-3 transverse momentum dependent (TMD) light-cone wave function  $\Phi_{\pi,P}$  and  $\Phi_{\pi,T}$  respectively[11, 22]. In the  $\pi\gamma^* \rightarrow \pi$  process we calculate, only the  $O(\alpha_s)$  order pseudoscalar component  $\Phi_{\pi,P}^{(1)}$  of the final state pion, but both the  $\Phi_{\pi,P}^{(1)}$  and  $\Phi_{\pi,T}^{(1)}$  components of the initial pion should be convoluted with the LO hard kernel.

$$\begin{aligned}
\Phi_{\pi,P}(x'_1, k'_{1T}; x_1, k_{1T}) = & \int \frac{dy^-}{2\pi} \frac{d^2 y_T}{(2\pi)^2} e^{-ix'_1 P_1^+ y^- + i\mathbf{k}'_{1T} \cdot \mathbf{y}_T} \\
& \cdot \langle 0 | \bar{q}(y) \gamma_5 W_y(n_1)^\dagger I_{n_1;y,0} W_0(n_1) q(0) | \bar{u}(P_1 - k_1) d(k_1) \rangle, \tag{33}
\end{aligned}$$

$$\begin{aligned}
\Phi_{\pi,T}(x'_1, k'_{1T}; x_1, k_{1T}) = & \int \frac{dy^-}{2\pi} \frac{d^2 y_T}{(2\pi)^2} e^{-ix'_1 P_1^+ y^- + i\mathbf{k}'_{1T} \cdot \mathbf{y}_T} \\
& \cdot \langle 0 | \bar{q}(y) \gamma_5 (\not{y}_+ \not{y}_- - 1) W_y(n_1)^\dagger I_{n_1;y,0} W_0(n_1) q(0) | \bar{u}(P_1 - k_1) d(k_1) \rangle, \tag{34}
\end{aligned}$$

$$\begin{aligned}
\Phi_{\pi,P}(x_2, k_{2T}; x'_2, k'_{2T}) = & \int \frac{dz^+}{2\pi} \frac{d^2 z_T}{(2\pi)^2} e^{-ix'_2 P_2^- z^+ + i\mathbf{k}'_{2T} \cdot \mathbf{z}_T} \\
& \cdot \langle 0 | \bar{q}(z) W_z(n_2)^\dagger I_{n_2;z,0} W_0(n_2) \gamma_5 q(0) | u(P_2 - k_2) \bar{d}(k_2) \rangle, \tag{35}
\end{aligned}$$

where  $y = (0, y^-, \mathbf{y}_T)$  and  $z = (z_+, 0, \mathbf{z}_T)$  are the light-cone coordinates of the anti-quark field  $\bar{q}$  carrying the momentum fraction  $x_i$ , respectively. The Wilson lines with the choice of  $n_i^2 \neq 0$  to

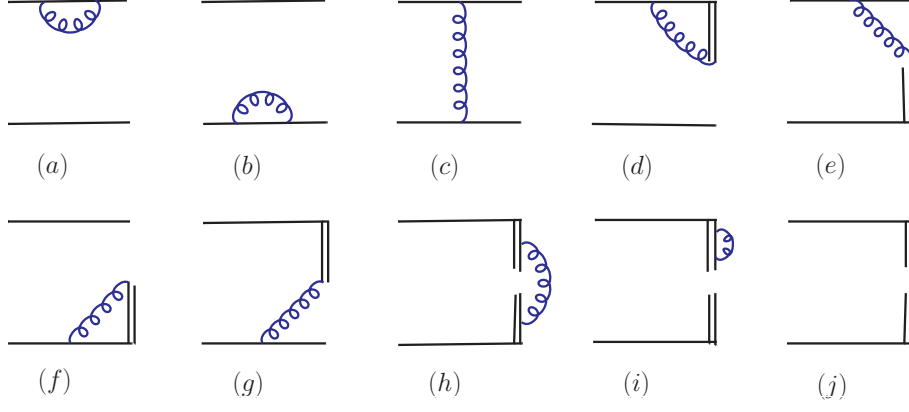


FIG. 5. The effective  $O(\alpha_s)$  diagrams for the initial  $\pi$  meson wave function.

avoid the light-cone singularity [10, 23] are defined as

$$W_y(n_1) = \text{P} \exp[-ig_s \int_0^\infty d\lambda n_1 \cdot A(y + \lambda n_1)], \quad (36)$$

$$W_z(n_2) = \text{P} \exp[-ig_s \int_0^\infty d\lambda n_1 \cdot A(z + \lambda n_2)], \quad (37)$$

where P is the path ordering operator. The two Wilson line  $W_y(n_i)$  ( $W_z(n_i)$ ) and  $W_0(n_i)$  are connected by a vertical link  $I_{n_i;y,0}$  ( $I_{n_i;z,0}$ ) at infinity [24]. Then the additional light-cone singularities from the region where loop momentum  $l \parallel n_-(n_+)$  [25] are regulated by the IR regulator  $n_1^2 \neq 0$  and  $n_2^2 \neq 0$ . The scales  $\xi_1^2 \equiv 4(n_1 \cdot p_1)^2 / |n_1^2| = Q^2 |n_1^- / n_1^+|$  and  $\xi_2^2 \equiv 4(n_2 \cdot p_2)^2 / |n_2^2| = Q^2 |n_2^+ / n_2^-|$  are introduced to decide the wave functions of the initial and final state pion respectively. It is important to emphasize that the variation of the above scales can be treated as a factorization scheme-dependence, which entered the hard kernel when taking the difference of the quark diagrams in full QCD and the effective diagrams for the wave functions in NLO calculations. Recently, the above scheme-dependent rapidity logarithms were diminished by joint resummation[26] for  $B$  meson wave functions[27], and for pion wave function and pion transition form factor[28]. In this paper we minimize the above scheme-dependent scales by adhering them to fixed  $n_1^2$  and  $n_2^2$ .

The convolution of the  $O(\alpha_s)$  initial state wave function as shown in Fig. 5 and  $H^{(0)}$  over the integration variables  $x'_1$  and  $k'_{1T}$  is of the form

$$\Phi_\pi^{(1)} \otimes H^{(0)} \equiv \int dx'_1 d^2 \mathbf{k}'_{1T} \Phi_\pi^{(1)}(x_1, \mathbf{k}_{1T}; x'_1, \mathbf{k}'_{1T}) H^{(0)}(x'_1, \mathbf{k}'_{1T}; x_2, \mathbf{k}_{2T}). \quad (38)$$

When making this convolution, the  $n_1$  is chosen approximately as the vector  $n_-$  with a very small plus component  $n_1^+$  to avoid the light-cone singularity. Note that the sign of  $n_1^-$  is positive while the sign of  $n_1^+$  can be positive or negative for convenience. The results after making the convolution

for each figure in Fig. 5 are given in the following with  $\mu_f$  being the factorization scale.

$$\begin{aligned}
\Phi_{5a}^{(1)} \otimes H^{(0)} &= -\frac{\alpha_s C_F}{8\pi} \left[ \frac{1}{\epsilon} + \ln \frac{4\pi\mu_f^2}{\delta_1 Q^2 e^{\gamma_E}} + 2 \right] H^{(0)}, \\
\Phi_{5b}^{(1)} \otimes H^{(0)} &= -\frac{\alpha_s C_F}{8\pi} \left[ \frac{1}{\epsilon} + \ln \frac{4\pi\mu_f^2}{\delta_1 Q^2 e^{\gamma_E}} + 2 \right] H^{(0)}, \\
\Phi_{5c}^{(1)} \otimes H^{(0)} &\equiv 0, \\
\Phi_{5d}^{(1)} \otimes H^{(0)} &= \frac{\alpha_s C_F}{8\pi} \left[ \frac{1}{\epsilon} + \ln \frac{4\pi\mu_f^2}{\xi_1^2 e^{\gamma_E}} - \ln^2(\delta_1 r_Q) - 2 \ln(\delta_1 r_Q) - \frac{\pi^2}{3} + 2 \right] H^{(0)}(x_1 p_1^\mu), \\
\Phi_{5e}^{(1)} \otimes H^{(0)} &= \frac{\alpha_s C_F}{8\pi} \left[ \ln^2\left(\frac{\delta_1 r_Q}{x_1}\right) + \pi^2 \right] H^{(0)}(x_1 p_1^\mu), \\
\Phi_{5f}^{(1)} \otimes H^{(0)} &= \frac{\alpha_s C_F}{8\pi} \left[ \frac{1}{\epsilon} + \ln \frac{4\pi\mu_f^2}{\xi_1^2 e^{\gamma_E}} - \ln^2\left(\frac{\delta_1 r_Q}{x_1^2}\right) - 2 \ln\left(\frac{\delta_1 r_Q}{x_1^2}\right) - \frac{\pi^2}{3} + 2 \right] H^{(0)}(p_2^\mu), \\
\Phi_{5g}^{(1)} \otimes H^{(0)} &= \frac{\alpha_s C_F}{8\pi} \left[ \ln^2\left(\frac{\delta_1 r_Q}{x_1^2}\right) - \frac{\pi^2}{3} \right] H^{(0)}(p_2^\mu), \\
(\Phi_{5h}^{(1)} + \Phi_{5i}^{(1)} + \Phi_{5j}^{(1)}) \otimes H^{(0)} &= \frac{\alpha_s C_F}{4\pi} \left[ \frac{1}{\epsilon} + \ln \frac{4\pi\mu_f^2}{Q^2 e^{\gamma_E}} - \ln \delta_{12} \right] H^{(0)}. \tag{39}
\end{aligned}$$

The dimensionless parameter  $r_Q = Q^2/\xi_1^2$  is defined to simplify the expressions as given in above equation. In Eq. (39) all the IR divergence are regulated by  $\ln \delta_1$  in the convolution  $\Phi_{\pi}^{(1)} \otimes H^{(0)}$ . Fig. 5(d,e) just give the corrections to the LO hard kernel  $H^{(0)}(x_1 p_1^\mu)$ , while Fig. 5(f,g) provide the corrections to the LO hard kernel  $H^{(0)}(p_2^\mu)$ , because the gluon attaches to the Wilson line and the up external line in the former two subdiagrams ( Fig. 5(d) and 5(e) ), but attaches to the Wilson line and the down external line in the later two subdiagrams ( Fig. 5(f) and 5(g) ). The corrections from Fig. 5(a,b) are canceled by those from Fig. 2(a,b). It is unnecessary to calculate the reducible subdiagram Fig. 5(c), since it will be canceled by Fig. 4(b) completely.

Only the three-point integral was involved in the convolution of  $\Phi_{5d}^{(1)} \otimes H^{(0)}$  and  $\Phi_{5f}^{(1)} \otimes H^{(0)}$ , because there is no momenta flow into the LO hard kernel in these two subdiagrams. A four-point integral should been calculated in the convolution  $\Phi_{5e}^{(1)} \otimes H^{(0)}$  because the momenta is flow into the LO hard kernel and the  $H^{(0)}(x_1 p_1^\mu)$  cancels an denominator. The convolution  $\Phi_{5g}^{(1)} \otimes H^{(0)}$  involves a five-point integral due to the flow momenta and the correction to the LO hard kernel  $H^{(0)}(p_2^\mu)$ . After summing up all  $O(\alpha_s)$  contributions in Fig. 5 except those from the reducible subdiagrams Fig. 5(a), 5(b) and 5(c), we find

$$\begin{aligned}
\Phi_{\pi}^{(1)} \otimes H^{(0)} &= \frac{\alpha_s C_F}{8\pi} \left[ \frac{3}{\epsilon} + 3 \ln \frac{4\pi}{e^{\gamma_E}} + 3 \ln \frac{\mu_f^2}{Q^2} - 2 \ln(\delta_1 r_Q)(\ln x_1 + 1) \right. \\
&\quad \left. - 2 \ln(x_1 x_2 r_Q) + \frac{2\pi^2}{3} - 2 \right] H^{(0)}(x_1 p_1^\mu) \\
&\quad + \frac{\alpha_s C_F}{8\pi} \left[ \frac{3}{\epsilon} + 3 \ln \frac{4\pi}{e^{\gamma_E}} + 3 \ln \frac{\mu_f^2}{Q^2} - 2 \ln(\delta_1 r_Q) \right. \\
&\quad \left. - 2 \ln(x_1 x_2 r_Q) + 4 \ln x_1 - \frac{2\pi^2}{3} - 2 \right] H^{(0)}(p_2^\mu), \tag{40}
\end{aligned}$$

where  $r_Q = Q^2/\xi_1^2$ .

The convolution of the LO hard kernel  $H^{(0)}$  and the NLO outgoing pion meson function  $\Phi_\pi^{(1)}$  over the integration variables  $x'_2$  and  $k'_{2T}$  is

$$H^{(0)} \otimes \Phi_\pi^{(1)} \equiv \int dx'_2 d^2 \mathbf{k}'_{2T} H^{(0)}(x_1, \mathbf{k}_{1T}; x'_2, \mathbf{k}'_{2T}) \Phi_{\pi,P}^{(1)}(x'_2, \mathbf{k}'_{2T}; x_2, \mathbf{k}_{2T}). \quad (41)$$

The unit vector  $n_2$  is chosen approximately as  $n_+$  with a very small minus component  $n_2^-$  to avoid the light-cone singularity in the convolution. Note that the sign of  $n_2^+$  is positive as  $P_1^+$  while the sign of  $n_2^-$  is arbitrary for convenience.

In Fig. 6 we draw all subdiagrams which provide  $\mathcal{O}(\alpha_s)$  NLO corrections to the outgoing pion wave functions. Analogous to the case of Fig. 5, we here make the same evolutions for all subdiagrams in Fig. 6. The analytical results for each subdiagram of Fig. 6 are listed in the following with  $\mu_f$  being the factorization scale.

$$\begin{aligned} H^{(0)} \otimes \Phi_{6a}^{(1)} &= -\frac{\alpha_s C_F}{8\pi} \left[ \frac{1}{\epsilon} + \ln \frac{4\pi\mu_f^2}{\delta_2 Q^2 e^{\gamma_E}} + 2 \right] H^{(0)}, \\ H^{(0)} \otimes \Phi_{6b}^{(1)} &= -\frac{\alpha_s C_F}{8\pi} \left[ \frac{1}{\epsilon} + \ln \frac{4\pi\mu_f^2}{\delta_2 Q^2 e^{\gamma_E}} + 2 \right] H^{(0)}, \\ H^{(0)} \otimes \Phi_{6c}^{(1)} &\equiv 0, \\ H^{(0)} \otimes \Phi_{6d}^{(1)} &= \frac{\alpha_s C_F}{8\pi} \left[ \frac{1}{\epsilon} + \ln \frac{4\pi\mu_f^2}{\xi_2^2 e^{\gamma_E}} - \ln^2(\delta_2 \gamma_Q) - 2 \ln(\delta_2 \gamma_Q) - \frac{\pi^2}{3} + 2 \right] H^{(0)}(x_1 p_1^\mu), \quad (42) \\ H^{(0)} \otimes \Phi_{6e}^{(1)} &= \frac{\alpha_s C_F}{8\pi} \left[ \ln^2\left(\frac{\delta_2 r_Q}{x_1}\right) + \pi^2 \right] H^{(0)}(x_1 p_1^\mu), \\ H^{(0)} \otimes \Phi_{6f}^{(1)} &= \frac{\alpha_s C_F}{8\pi} \left[ \frac{1}{\epsilon} + \ln \frac{4\pi\mu_f^2}{\xi_2^2 e^{\gamma_E}} - \ln^2\left(\frac{\delta_2 r_Q}{x_2^2}\right) - 2 \ln\left(\frac{\delta_2 r_Q}{x_2^2}\right) - \frac{\pi^2}{3} + 2 \right] H^{(0)}(p_2^\mu), \\ H^{(0)} \otimes \Phi_{6g}^{(1)} &= \frac{\alpha_s C_F}{8\pi} \left[ \ln^2\left(\frac{\delta_2 r_Q}{x_2^2}\right) - \frac{\pi^2}{3} \right] H^{(0)}(p_2^\mu), \\ H^{(0)} \otimes (\Phi_{6h}^{(1)} + \Phi_{6i}^{(1)} + \Phi_{6j}^{(1)}) &= \frac{\alpha_s C_F}{4\pi} \left[ \frac{1}{\epsilon} + \ln \frac{4\pi\mu_f^2}{Q^2 e^{\gamma_E}} - \ln \delta_{12} \right] H^{(0)}, \quad (43) \end{aligned}$$

where  $r_Q = Q^2/\xi_1^2$ . The most complex integral involved in our calculation for Fig. 6 is the four-point integral, since the relevant momentum fraction  $x'_2$  is only appeared in one propagator in the LO hard kernel  $H^{(0)}$ .

The total contributions from the convolution of the LO hard kernel  $H^{(0)}$  and the NLO final pion meson wave function is obtained by summing up all contributions as listed in above equation, and we dropped the contributions from those reducible subdiagrams  $G^{(1)}(a, b, c)$ . The summation from all irreducible subdiagrams of Fig. 6 leads to the final result:

$$\begin{aligned} H^{(0)} \otimes \Phi_\pi^{(1)} &= \frac{\alpha_s C_F}{8\pi} \left[ \frac{3}{\epsilon} + 3 \ln \frac{4\pi}{e^{\gamma_E}} + 3 \ln \frac{\mu_f^2}{Q^2} - 2 \ln(\delta_2 r_Q)(\ln x_2 + 1) \right. \\ &\quad \left. - 2 \ln(x_1 x_2 r_Q) + \frac{2\pi^2}{3} - 2 \right] H^{(0)}(x_1 p_1^\mu) \\ &\quad + \frac{\alpha_s C_F}{8\pi} \left[ \frac{3}{\epsilon} + 3 \ln \frac{4\pi}{e^{\gamma_E}} + 3 \ln \frac{\mu_f^2}{Q^2} - 2 \ln(\delta_2 r_Q) \right. \\ &\quad \left. - 2 \ln(x_1 x_2 r_Q) + 4 \ln x_2 - \frac{2\pi^2}{3} - 2 \right] H^{(0)}(p_2^\mu), \quad (44) \end{aligned}$$

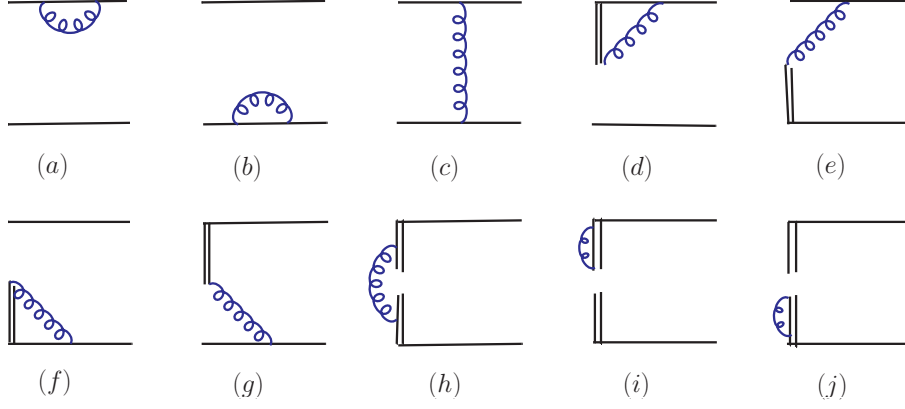


FIG. 6. The  $O(\alpha_s)$  subdiagrams for the final  $\pi$  meson wave function.

where  $r_Q = Q^2/\xi_1^2$ .

### C. The NLO twist-3 Hard Kernel

The IR-finite  $k_T$  dependent NLO twist-3 hard kernel for the  $\pi\gamma^* \rightarrow \pi$  form factor is derived by taking the difference between the contributions from the quark diagrams in full QCD and the contributions from the effective diagrams for pion wave functions [29].

$$\begin{aligned}
 H^{(1)}(x_1, \mathbf{k}_{1T}; x_2, \mathbf{k}_{2T}) &= G^{(1)}(x_1, \mathbf{k}_{1T}; x_2, \mathbf{k}_{2T}) \\
 &- \int dx'_1 d^2\mathbf{k}'_{1T} \Phi_\pi^{(1)}(x_1, \mathbf{k}_{1T}; x'_1, \mathbf{k}'_{1T}) H^{(0)}(x'_1, \mathbf{k}'_{1T}; x_2, \mathbf{k}_{2T}) \\
 &- \int dx'_2 d^2\mathbf{k}'_{2T} H^{(0)}(x_1, \mathbf{k}_{1T}; x'_2, \mathbf{k}'_{2T}) \Phi_{\pi,P}^{(1)}(x'_2, \mathbf{k}'_{2T}; x_2, \mathbf{k}_{2T}), \tag{45}
 \end{aligned}$$

where  $\Phi_\pi^{(1)}(x_1, \mathbf{k}_{1T}; x'_1, \mathbf{k}'_{1T})$  include two parts:  $\Phi_{\pi,P}^{(1)}(x_1, \mathbf{k}_{1T}; x'_1, \mathbf{k}'_{1T})$  and  $\Phi_{\pi,T}^{(1)}(x_1, \mathbf{k}_{1T}; x'_1, \mathbf{k}'_{1T})$ .

The bare coupling constant  $\alpha_s$  in Eq. (32,40,44) can be rewritten as

$$\alpha_s = \alpha_s(\mu_f) + \delta Z(\mu_f) \alpha_s(\mu_f), \tag{46}$$

in which the counterterm  $\delta Z(\mu_f)$  is defined in the modified minimal subtraction scheme. Inserting Eq. (46) into Eq. (10,32,40,44) regularizes the UV poles in Eq. (45) through the term  $\delta Z(\mu_f) H^{(0)}$ , and then the UV poles in Eq. (40,44) are regulated by the counterterm of the quark field and by an additional counterterm in the modified minimal subtraction scheme. The UV behavior of the NLO twist-3 contributions is the same as the NLO twist-2 ones, which satisfy the requirement of the universality of the pion wave functions.

Based on the above calculations, it is straightforward to write down the NLO twist-3 hard kernel



$H^{(1)}$  for Fig. 1(a), assuming  $\xi_1^2 \equiv \xi_2^2 \equiv Q^2$ :

$$\begin{aligned}
H^{(1)} = & \frac{\alpha_s(\mu_f)C_F}{8\pi} \left[ \frac{21}{2} \ln \frac{\mu^2}{Q^2} - 6 \ln \frac{\mu_f^2}{Q^2} - \frac{53}{8} \ln(x_1 x_2) \right. \\
& - \frac{23}{8} \ln x_1 - \frac{4}{9} \ln x_2 - \frac{1}{4} \ln^2 x_2 - \frac{137}{48} \pi^2 + \frac{337}{32} \left. \right] H^{(0)}(x_1 p_1^\mu) \\
& + \frac{\alpha_s(\mu_f)C_F}{8\pi} \left[ \frac{21}{2} \ln \frac{\mu^2}{Q^2} - 6 \ln \frac{\mu_f^2}{Q^2} - 8 \ln(x_1 x_2) \right. \\
& \left. - \ln x_1 + 4 \ln x_2 - \frac{31}{12} \pi^2 + \frac{1}{2} \ln 2 + 11 \right] H^{(0)}(p_2^\mu), \tag{47}
\end{aligned}$$

where  $\mu$  and  $\mu_f$  are the renormalization scale and factorization scale respectively. Following the schemes in the NLO analysis of the  $B \rightarrow \pi$  transition form factor at the leading twist [10], we here also set  $\xi_2^2 = Q^2$  in order to obtain a simple expression as given in Eq. (47).

The additional double logarithm  $\ln^2 x_1$ , derived from the limit that the internal quark is on-shell due to the tiny momentum fraction  $x_1$ , should also be considered. It can be absorbed into the Jet function  $J(x_1)$  as in Refs. [14, 15]

$$J^{(1)} H^{(0)} = -\frac{1}{2} \frac{\alpha_s(\mu_f)C_F}{4\pi} \left[ \ln^2 x_1 + \ln x_1 + \frac{\pi^2}{3} \right] H^{(0)}(p_2^\mu), \tag{48}$$

where the factor  $\frac{1}{2}$  reflects the different spin structure of the twist-3 and twist-2 parts. There exists no Jet function  $J(x_2)$  because the momentum fraction  $x_2$  wouldn't grow end-point singularity. The NLO twist-3 hard kernel  $H^{(1)}$  in Eq. (47) will become the following form after subtracting out the Jet function in Eq. (48)

$$\begin{aligned}
H^{(1)}(x_i, \mu, \mu_f, Q^2) & \rightarrow H^{(1)} - J^{(1)} H^{(0)} \\
& \equiv F_{\text{T3,A1}}^{(1)}(x_i, \mu, \mu_f, Q^2) H^{(0)}(x_1 p_1^\mu) + F_{\text{T3,A2}}^{(1)}(x_i, \mu, \mu_f, Q^2) H^{(0)}(p_2^\mu), \tag{49}
\end{aligned}$$

where the two factors of the NLO twist-3 contributions for Fig.1(a) are of the form

$$\begin{aligned}
F_{\text{T3,A1}}^{(1)}(x_i, \mu, \mu_f, Q^2) = & \frac{\alpha_s(\mu_f)C_F}{8\pi} \left[ \frac{21}{2} \ln \frac{\mu^2}{Q^2} - 6 \ln \frac{\mu_f^2}{Q^2} - \frac{53}{8} \ln(x_1 x_2) \right. \\
& \left. - \frac{23}{8} \ln x_1 - \frac{4}{9} \ln x_2 - \frac{1}{4} \ln^2 x_2 - \frac{137}{48} \pi^2 + \frac{337}{32} \right], \tag{50}
\end{aligned}$$

$$\begin{aligned}
F_{\text{T3,A2}}^{(1)}(x_i, \mu, \mu_f, Q^2) = & \frac{\alpha_s(\mu_f)C_F}{8\pi} \left[ \frac{21}{2} \ln \frac{\mu^2}{Q^2} - 6 \ln \frac{\mu_f^2}{Q^2} - 8 \ln(x_1 x_2) \right. \\
& \left. + \ln^2 x_1 + 4 \ln x_2 - \frac{27}{12} \pi^2 + \frac{1}{2} \ln 2 + 11 \right]. \tag{51}
\end{aligned}$$

The IR-finite and  $k_T$  dependent NLO hard kernel  $H^{(1)}(\mu, \mu_f, x_i, Q^2)$  as given in Eq. (49) describe the NLO twist-3 contribution to the LO twist-3 hard kernel  $H_a^{(0)}$  as given in Eq. (6) for the Fig.1(a). One can obtain the NLO twist-3 corrections to the LO twist-3 hard kernel  $H_b^{(0)}$ ,  $H_c^{(0)}$  and  $H_d^{(0)}$  for other three subdiagrams Fig.1(b), 1(c) and 1(d) respectively, by simple replacements. For Fig. 1(b), for example, the two factors of the NLO twist-3 contributions  $F_{\text{T3,B1}}^{(1)}(x_i, \mu, \mu_f, Q^2)$

and  $F_{\text{T3,B2}}^{(1)}(x_i, \mu, \mu_f, Q^2)$  can be obtained from those in Eqs. (50,51) by simple replacements  $x_1 \longleftrightarrow x_2$ :

$$F_{\text{T3,B1}}^{(1)}(x_i, \mu, \mu_f, Q^2) = \frac{\alpha_s(\mu_f)C_F}{8\pi} \left[ \frac{21}{2} \ln \frac{\mu^2}{Q^2} - 6 \ln \frac{\mu_f^2}{Q^2} - \frac{53}{8} \ln(x_1 x_2) - \frac{23}{8} \ln x_2 - \frac{4}{9} \ln x_1 - \frac{1}{4} \ln^2 x_1 - \frac{137}{48} \pi^2 + \frac{337}{32} \right], \quad (52)$$

$$F_{\text{T3,B2}}^{(1)}(x_i, \mu, \mu_f, Q^2) = \frac{\alpha_s(\mu_f)C_F}{8\pi} \left[ \frac{21}{2} \ln \frac{\mu^2}{Q^2} - 6 \ln \frac{\mu_f^2}{Q^2} - 8 \ln(x_1 x_2) + \ln^2 x_2 + 4 \ln x_1 - \frac{27}{12} \pi^2 + \frac{1}{2} \ln 2 + 11 \right]. \quad (53)$$

We can also obtain the factors  $F_{\text{T3,C1}}^{(1)}$  and  $F_{\text{T3,C2}}^{(1)}$  for subdiagrams Fig.1(c) by the replacements:  $x_1 \rightarrow \bar{x}_1 = 1 - x_1$  and  $x_2 \rightarrow \bar{x}_2 = 1 - x_2$  from Eqs. (50,51). For Fig. 1(d), finally, one finds the factors  $F_{\text{T3,D1}}^{(1)}$  and  $F_{\text{T3,D2}}^{(1)}$  from those in Eqs. (50,51) by the replacements:  $x_1 \rightarrow \bar{x}_2$  and  $x_2 \rightarrow \bar{x}_1$ .

#### IV. NUMERICAL ANALYSIS

In this section, by employing the  $k_T$  factorization theorem, we will calculate the pion electromagnetic form factor  $F^+(q^2)$  of the  $\pi\gamma^* \rightarrow \pi$  process numerically. Besides the LO twist-2 and twist-3 contributions, the NLO twist-2 contribution as given in Ref. [9] and the NLO twist-3 contributions evaluated in this paper are all taken into account. We will compare the relative strength of the four parts numerically.

In order to compare our results directly with the theoretical predictions for the LO twist-2, LO twist-3 and NLO twist-2 contributions to pion form factor as presented in Ref. [9], we here firstly consider two different choices for the pion distribution amplitudes (DA's): Set-A: the simple asymptotic pion DA's:

$$\phi_\pi^A(x) = \frac{3f_\pi}{\sqrt{6}}x(1-x), \quad \phi_\pi^P(x) = \frac{f_\pi}{2\sqrt{6}}, \quad \phi_\pi^T(x) = \frac{f_\pi}{2\sqrt{6}}(1-2x); \quad (54)$$

with the pion decay constant  $f_\pi = 0.13$  GeV; and Set-B: the nonasymptotic pion DA's the same as those given in Eq. (39) of Ref. [9]:

$$\begin{aligned} \phi_\pi^A(x) &= \frac{3f_\pi}{\sqrt{6}}x(1-x) \left[ 1 + 0.16C_2^{\frac{3}{2}}(u) + 0.04C_4^{\frac{3}{2}}(u) \right], \\ \phi_\pi^P(x) &= \frac{f_\pi}{2\sqrt{6}} \left[ 1 + 0.59C_2^{\frac{1}{2}}(u) + 0.09C_4^{\frac{1}{2}}(u) \right], \\ \phi_\pi^T(x) &= \frac{f_\pi}{2\sqrt{6}}(1-2x) \left[ 1 + 0.019(1-10x+10x^2) \right], \end{aligned} \quad (55)$$

where  $u = 1 - 2x$ , the Gegenbauer polynomials  $C_{2,4}^{1/2,3/2}(u)$  can be found easily in Refs. [19, 30].

In order to check the variations of the theoretical predictions induced by using different nonasymptotic pion DA's, we also consider the third choice of pion DA's: Set-C: the pion DA's

popularly used in recent years, for example, in Refs.[31–33]:

$$\begin{aligned}\phi_\pi^A(x) &= \frac{3f_\pi}{\sqrt{6}}x(1-x) \left[ 1 + a_2^\pi C_2^{\frac{3}{2}}(u) + a_4^\pi C_4^{\frac{3}{2}}(u) \right], \\ \phi_\pi^P(x) &= \frac{f_\pi}{2\sqrt{6}} \left[ 1 + \left( 30\eta_3 - \frac{5}{2}\rho_\pi^2 \right) C_2^{\frac{1}{2}}(u) - 3 \left( \eta_3\omega_3 + \frac{9}{20}\rho_\pi^2 (1 + 6a_2^\pi) \right) C_4^{\frac{1}{2}}(u) \right], \\ \phi_\pi^T(x) &= \frac{f_\pi}{2\sqrt{6}}(1-2x) \left[ 1 + 6 \left( 5\eta_3 - \frac{1}{2}\eta_3\omega_3 - \frac{7}{20}\rho_\pi^2 - \frac{3}{5}\rho_\pi^2 a_2^\pi \right) (1 - 10x + 10x^2) \right],\end{aligned}\quad (56)$$

where the Gegenbauer moments  $a_i^\pi$ , the parameters  $\eta_3, \omega_3$  and  $\rho_\pi$  are adopted from Refs. [19, 30, 31]:

$$a_2^\pi = 0.25, \quad a_4^\pi = -0.015, \quad \rho_\pi = m_\pi/m_0, \quad \eta_3 = 0.015, \quad \omega_3 = -3.0, \quad (57)$$

with  $m_\pi = 0.13$  GeV,  $m_0 = 1.74$  GeV. It is easy to see that the asymptotic pion DA's in Eq. (54) are just the first (leading) term of the nonasymptotic pion DA's as given in Eq. (55) and Eq. (56). We will make numerical calculations by employing these three sets of pion DA's respectively, for the sake of comparison and for the examination of the effects of the shape of the pion DA's.

When both the LO twist-2 and LO twist-3 contributions are included, the LO form factor for  $\pi\gamma^* \rightarrow \pi$  process can be written as [9, 34],

$$\begin{aligned}F^+(Q^2)|_{\text{LO}} &= \frac{8}{9}\pi Q^2 \int dx_1 dx_2 \int b_1 db_1 b_2 db_2 \\ &\cdot \left\{ x_1 \phi_\pi^A(x_1) \phi_\pi^A(x_2) - 2r_\pi^2 \phi_\pi^P(x_2) [(x_1 - 1)\phi_\pi^P(x_1) + (x_1 + 1)\phi_\pi^T(x_1)] \right\} \\ &\cdot \alpha_s(t) \cdot e^{-2S_\pi(t)} \cdot S_t(x_2) \cdot h(x_1, x_2, b_1, b_2),\end{aligned}\quad (58)$$

where  $r_\pi^2 = m_0^2/Q^2$ , the first term  $x_1 \phi_\pi^A(x_1) \phi_\pi^A(x_2)$  leads to the LO twist-2 contribution, while the second term in the large bracket provide the LO twist-3 part. The  $k_T$  resummation factor  $S_\pi(t)$  is adopted from Ref. [34, 35]

$$S_\pi(\mu, b_i) = s(x_i \frac{Q}{\sqrt{2}}, b_i) + s(\bar{x}_i \frac{Q}{\sqrt{2}}, b_i) + 2 \int_{1/b_i}^\mu \frac{d\bar{\mu}}{\bar{\mu}} r_Q(g(\bar{\mu})), \quad (59)$$

with  $i = 1, 2$  for the initial and final  $\pi$  meson respectively. The expressions of the function  $s(Q', b)$  and the anomalous dimension  $\gamma_q$  can be found in Ref. [35]. The threshold resummation factor  $S_t(x)$  in Eq. (58) is adopted from Ref. [12]

$$S_t(x) = \frac{2^{1+2c}\Gamma(3/2+c)}{\sqrt{\pi}\Gamma(1+c)}[x(1-x)]^c, \quad (60)$$

and we here set the parameter  $c = 0.3$ . The hard function  $h(x_1, x_2, b_1, b_2)$  in Eq. (58) comes from the Fourier transformation and can be written as [9]

$$\begin{aligned}h(x_1, x_2, b_1, b_2) &= K_0(\sqrt{x_1 x_2} Q b_1) \left[ \theta(b_1 - b_2) I_0(\sqrt{x_2} Q b_2) K_0(\sqrt{x_2} Q b_1) \right. \\ &\quad \left. + \theta(b_2 - b_1) I_0(\sqrt{x_2} Q b_1) K_0(\sqrt{x_2} Q b_2) \right],\end{aligned}\quad (61)$$

where  $J_0$  is the Bessel function, and  $K_0, K_1$  and  $I_0$  are modified Bessel functions.

According to the discussions as presented in Ref. [9], we get to know that the relative strength of the NLO twist-2 contribution to the LO twist-2 one has a moderate dependence on the choice of

the renormalization scale  $\mu$ , the factorization scale  $\mu_f$  and the hard scale  $t$ . One can see from the curves in the Fig. 6 of Re. [9] that when one adopt the conventional choice of the scales [5], i.e.,

$$\mu = \mu_f = t = \max(\sqrt{x_1}Q, \sqrt{x_2}Q, 1/b_1, 1/b_2), \quad (62)$$

where the hard scale  $t$  is the largest energy scale in Fig. 1, the NLO twist-2 correction becomes less than 40% of the LO twist-2 contribution as  $Q^2 > 7 \text{ GeV}^2$ , or less than 20% of the total LO contribution. This means that such choice can minimize the NLO twist-2 correction to the form factors in consideration. We here also make the same choices as given in Eq. (62) in our numerical calculations of the NLO twist-2 and twist-3 contributions. For more details about the choice of  $\mu$ ,  $\mu_f$  and hard scale  $t$ , one can see Ref. [9].

When the LO twist-2, LO twist-3, NLO twist-2 and NLO twist-3 contributions to the pion form factors are all taken into account, the pion form factor  $F^+(q^2)$  for  $\pi\gamma^* \rightarrow \pi$  process in the  $k_T$  factorization can be written as

$$\begin{aligned} F^+(Q^2)|_{\text{NLO}} = & \frac{8}{9}\pi Q^2 \int dx_1 dx_2 \int b_1 db_1 b_2 db_2 \cdot \left\{ x_1 \phi_\pi^A(x_1) \phi_\pi^A(x_2) \cdot \left[ 1 + F_{\text{T2}}^{(1)}(x_i, t, Q^2) \right] \right. \\ & - 2r_\pi^2 x_1 \phi_\pi^P(x_2) \left[ 1 + F_{\text{T3}}^{(1)}(x_i, t, Q^2) \right] (\phi_\pi^P(x_1) + \phi_\pi^T(x_1)) \\ & + 2r_\pi^2 \phi_\pi^P(x_2) \left[ 1 + \bar{F}_{\text{T3}}^{(1)}(x_i, t, Q^2) \right] \cdot (\phi_\pi^P(x_1) - \phi_\pi^T(x_1)) \left. \right\} \\ & \cdot \alpha_s(t) \cdot e^{-2S_\pi(t)} \cdot S_t(x_2) \cdot h(x_1, x_2, b_1, b_2) \end{aligned} \quad (63)$$

where the factor  $F_{\text{T2}}^{(1)}(x_i, t, Q^2)$  denotes the NLO twist-2 contribution as given in Ref. [9]

$$\begin{aligned} F_{\text{T2}}^{(1)}(x_i, t, Q^2) = & \frac{\alpha_s(t)C_F}{4\pi} \left[ -\frac{3}{4} \ln \frac{t^2}{Q^2} - \ln^2 x_1 - \ln^2 x_2 + \frac{45}{8} \ln x_1 \ln x_2 \right. \\ & \left. + \frac{5}{4} \ln x_1 + \frac{77}{16} \ln x_2 + \frac{1}{2} \ln 2 + \frac{5}{48} \pi^2 + \frac{53}{4} \right]. \end{aligned} \quad (64)$$

The factor  $F_{\text{T3}}^{(1)}(x_i, t, Q^2)$  and  $\bar{F}_{\text{T3}}^{(1)}(x_i, t, Q^2)$  in Eq. (63) describe the NLO twist-3 contributions and have been defined in Eqs. (50,51). By making the same choice of scales ( $\mu, \mu_f, t$ ) as the one in Eq. (62), these two factors become relatively simple

$$\begin{aligned} F_{\text{T3}}^{(1)}(x_i, t, Q^2) = & \frac{\alpha_s(t)C_F}{4\pi} \left[ \frac{9}{4} \ln \frac{t^2}{Q^2} - \frac{53}{16} \ln x_1 x_2 - \frac{23}{16} \ln x_1 \right. \\ & \left. - \frac{2}{9} \ln x_2 - \frac{1}{8} \ln^2 x_2 - \frac{137}{96} \pi^2 + \frac{337}{64} \right], \end{aligned} \quad (65)$$

$$\begin{aligned} \bar{F}_{\text{T3}}^{(1)}(x_i, t, Q^2) = & \frac{\alpha_s(t)C_F}{4\pi} \left[ \frac{9}{4} \ln \frac{t^2}{Q^2} - 4 \ln(x_1 x_2) + \frac{1}{2} \ln^2 x_1 \right. \\ & \left. + 2 \ln x_2 - \frac{27}{24} \pi^2 + \frac{1}{4} \ln 2 + \frac{11}{2} \right]. \end{aligned} \quad (66)$$

By using the three sets of pion distribution amplitudes  $\phi_\pi^{A,P,T}(x)$  as given in Eqs. (54), (55) and Eq. (56) respectively, and fixing the scales as in Eq.(62), we calculate the four different LO and NLO contributions to the pion form factors and show the theoretical predictions in Table I and II, and in Figs. 7-10, respectively.

In Table I, we list the theoretical predictions for the four kinds of contributions: the LO twist-2, LO twist-3, NLO twist-2 and NLO twist-3 contributions to the pion form factors  $Q^2 F^+(Q^2)$

TABLE I. The theoretical predictions for contributions to  $Q^2 F^+(Q^2)$  from different orders and twists, for  $Q^2 = (1, 3, 5, 7, 10, 100)$  GeV<sup>2</sup> and for different cases: i.e., using different sets of pion DA's respectively.

$Q^2 F^+(Q^2)$	DA's	1	3	5	7	10	100
LO T-2	Set-A	0.078	0.070	0.080	0.085	0.089	0.086
	Set-B	0.075	0.075	0.086	0.093	0.098	0.109
	Set-C	0.071	0.076	0.089	0.095	0.102	0.116
NLO-T2	Set-A	0.102	0.039	0.035	0.034	0.033	0.022
	Set-B	0.106	0.044	0.040	0.039	0.037	0.030
	Set-C	0.106	0.047	0.043	0.041	0.040	0.033
LO-T3	Set-A	0.399	0.141	0.099	0.076	0.056	0.007
	Set-B	0.905	0.558	0.491	0.447	0.405	0.207
	Set-C	0.519	0.206	0.145	0.113	0.087	0.010
NLO-T3	Set-A	-0.252	-0.059	-0.037	-0.028	-0.021	-0.003
	Set-B	-0.261	-0.155	-0.151	-0.148	-0.144	-0.104
	Set-C	-0.286	-0.073	-0.046	-0.034	-0.025	-0.002
Full LO	Set-A	0.476	0.211	0.179	0.160	0.145	0.092
	Set-B	0.981	0.633	0.571	0.540	0.504	0.316
	Set-C	0.590	0.282	0.234	0.209	0.189	0.126
LO+NLO	Set-A	0.326	0.190	0.176	0.166	0.156	0.111
	Set-B	0.825	0.522	0.466	0.431	0.397	0.242
	Set-C	0.409	0.256	0.230	0.216	0.204	0.157

for fixed values of  $Q^2 = (1, 3, 5, 7, 10, 100)$  GeV<sup>2</sup>. In the numerical calculations, three sets of different choices of pion DA's are used respectively, with the labels of Set-A, Set-B and Set-C.

In order to compare the relative strength of different contributions directly we define the following four ratios:

$$\begin{aligned}
 R_1 &= \frac{F_{\text{NLO-T2}}^+(Q^2)}{F_{\text{LO-T2}}^+(Q^2)}, & R_2 &= \frac{F_{\text{NLO-T3}}^+(Q^2)}{F_{\text{LO-T3}}^+(Q^2)}, \\
 R_3 &= \frac{F_{\text{NLO}}^+(Q^2)}{F_{\text{LO}}^+(Q^2)}, & R_4 &= \frac{F_{\text{NLO}}^+(Q^2)}{F_{\text{NLO}}^+(Q^2) + F_{\text{LO}}^+(Q^2)},
 \end{aligned} \tag{67}$$

where  $R_1$  ( $R_2$ ) measures the ratio between NLO twist-2 (twist-3) and LO twist-2 (twist-3) contribution,  $R_3$  describes the relative strength between the NLO contribution and the LO ones, and finally  $R_4$  is the ratio of the NLO contribution over the total contribution: all four parts, LO plus NLO contributions. In Table II, we present the numerical values of the ratios of the different kind of contributions to  $F^+(Q^2)$  for fixed values of  $Q^2 = (1, 3, 5, 7, 10, 100)$  GeV<sup>2</sup> and for three different sets of the pion DA's, respectively.

In Fig. 7, we show the  $Q^2$ -dependence of the various contributions to the pion form factors from different orders and twists for  $1 \leq Q^2 \leq 100$  GeV<sup>2</sup>, by using the asymptotic pion DA's as given in Eq. (54) and setting  $\mu = \mu_f = t$ . The Fig. 7(b) shows the enlargement of Fig. 7(a) in the low- $Q^2$  region:  $1 \leq Q^2 \leq 10$  GeV<sup>2</sup>. The experimental data shown in Fig. 7(b) are taken from Refs. [36, 37]. The Fig. 8 and Fig. 9 also show the  $Q^2$ -dependence of the various contributions

TABLE II. The ratios of the different contributions or their combinations as defined in Eq. (67), for  $Q^2 = (1, 3, 5, 7, 10, 100)$  GeV<sup>2</sup> respectively.

Ratios	DA's	1	3	5	7	10	100
$R_1$	Set-A	1.303	0.549	0.440	0.398	0.367	0.256
	Set-B	1.406	0.595	0.467	0.418	0.382	0.273
	Set-C	1.488	0.616	0.481	0.430	0.393	0.284
$R_2$	Set-A	-0.633	-0.423	-0.376	-0.368	-0.372	-0.487
	Set-B	-0.288	-0.277	-0.307	-0.331	-0.356	-0.503
	Set-C	-0.552	-0.356	-0.319	-0.302	-0.288	-0.199
$R_3$	Set-A	-0.316	-0.099	-0.012	0.036	0.080	0.203
	Set-B	-0.158	-0.174	-0.191	-0.202	-0.212	-0.235
	Set-C	-0.306	-0.094	-0.016	0.032	0.080	0.247
$R_4$	Set-A	-0.462	-0.110	-0.013	0.035	0.074	0.169
	Set-B	-0.188	-0.211	-0.237	-0.254	-0.269	-0.307
	Set-C	-0.441	-0.103	-0.016	0.031	0.074	0.198

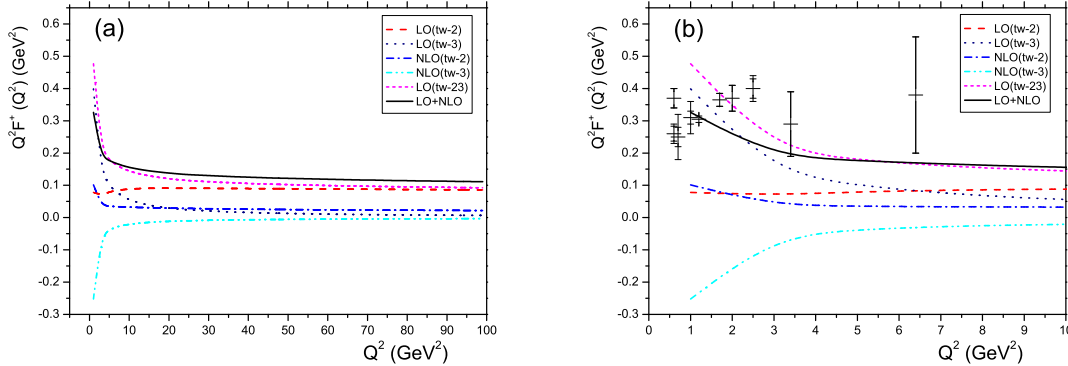


FIG. 7. Contributions to  $Q^2 F^+(Q^2)$  from different orders and twists, using the asymptotic pion DA's as given in Eq. (54). Figure 7(a) shows the  $Q^2$ -dependence for  $1 \leq Q^2 \leq 100$  GeV<sup>2</sup>, while 7(b) is the enlargement of 7(a) in the low- $Q^2$  region:  $1 \leq Q^2 \leq 10$  GeV<sup>2</sup>. The experiment data in 7(b) are taken from Refs. [36, 37].

to the pion form factors, but using the nonasymptotic pion DA's as given in Eqs. (55,56) instead of the asymptotic ones in Eq.(54). In Fig. 10, we show the  $Q^2$ -dependence of the four ratios  $R_{1,2}$  and  $R_{3,4}$  for  $1 \leq Q^2 \leq 100$  GeV<sup>2</sup>, assuming  $c = 0.3$  and  $\mu = \mu_f = t$  and employing the three different sets of the pion DA's.

From the theoretical predictions for the pion form factors from different orders and twists, as listed in Table I and II, and illustrated in Fig. 7-10, one can have the following observations:

- (i) For the LO twist-2 and NLO twist-2 contributions to the pion form factors  $F^+(Q^2)$  obtained in this work agree very well with those presented in Ref. [9] when the same Set-A and Set-B pion DA's are used, as can be seen easily from the numerical results in Table I and II, as

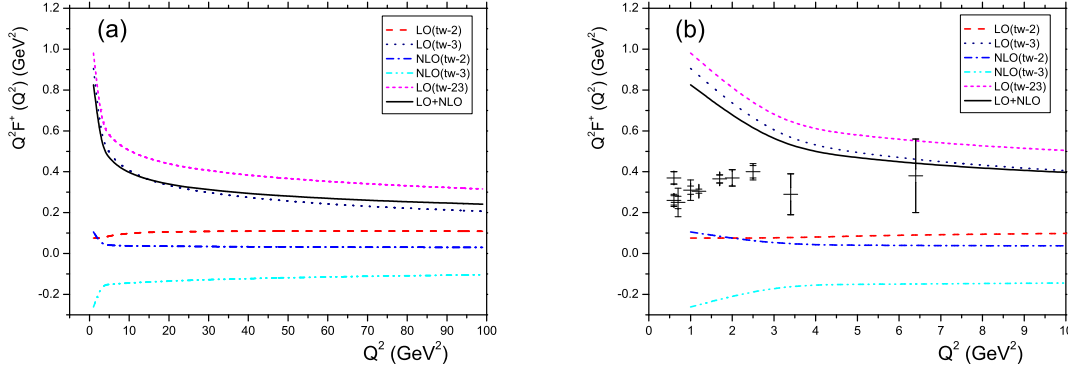


FIG. 8. The same as Fig. 7, but using the nonasymptotic pion DA's as given in Eq. (55).

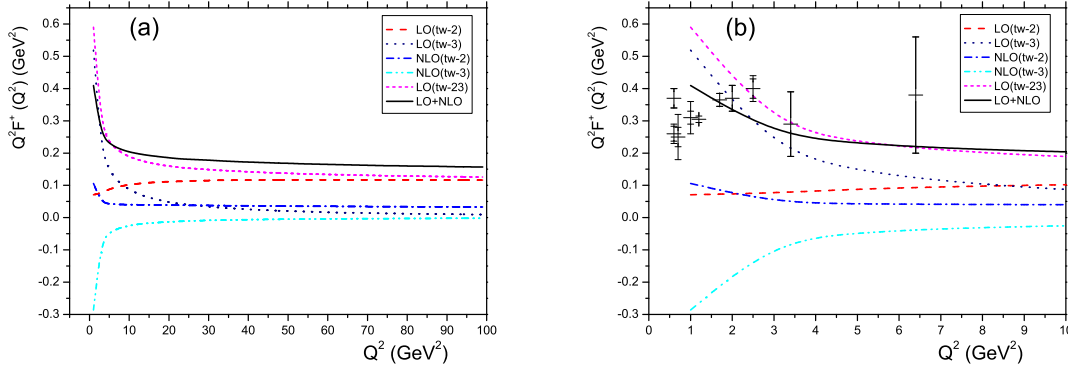


FIG. 9. The same as Fig. 7, but using the nonasymptotic pion DA's as given in Eq. (56).

well as in the Figs. 7-9. Even when the Set-C pion DA's as given in Eq. (56) were used, the theoretical predictions for the LO twist-2 and NLO twist-2 contributions are still well consistent with those in Ref. [9], since the twist-2  $\phi_\pi^A(x)$  in Eq. (55) and Eq. (56) have a little difference only. By using  $a_2^\pi = 0.25$  and  $a_4^\pi = -0.015$ , we find from Eq. (56) directly that

$$\phi_\pi^A(x) = \frac{f_\pi}{2\sqrt{6}} \left[ 1 + 0.25 C_2^{\frac{3}{2}}(u) - 0.015 C_4^{\frac{3}{2}}(u) \right]. \quad (68)$$

The coefficient of the second term is  $a_2^\pi = 0.25$ , close to the 0.16 in the  $\phi_\pi^A(x)$  in Eq. (55).

- (ii) For the LO twist-3 and NLO twist-3 contributions, one can see from the numerical results in Table I and the curves in Figs. 7-9 that these two contributions are rather similar with each other in both the magnitude and the shape when Set-A and Set-C pion DA's are used, respectively. When the Set-B pion DA's as given in Eq. (55) are employed, however, the corresponding theoretical predictions for both the LO twist-3 and NLO twist-3 contributions become rather different from those obtained by using the Set-C pion DA's. The reason is that there is a clear difference for the twist-3 DA's  $\phi_\pi^P(x)$  and  $\phi_\pi^T(x)$  in Eq. (55) and Eq. (56), specifically for  $\phi_\pi^T(x)$ . Using the Gegenbauer moments and other input parameters as given



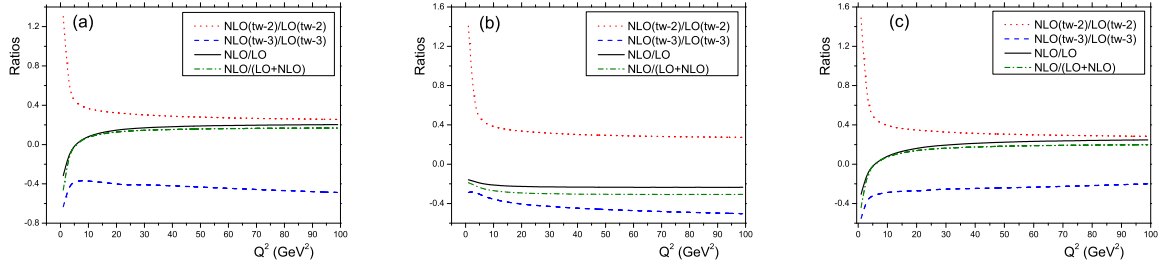


FIG. 10. Ratios of the NLO corrections over the LO contributions to the pion form factor, assuming  $\mu = \mu_f = t$ . (a) the asymptotic pion DA's in Eq. (54) are used; (b) the nonasymptotic DA's in Eq.(55) are used; and (c) the nonasymptotic DA's in Eq.(56) are used.

in Eq. (57), we find numerically that

$$\begin{aligned}\phi_\pi^P(x) &= \frac{f_\pi}{2\sqrt{6}} \left[ 1 + 0.43 C_2^{\frac{1}{2}}(u) + 0.11 C_4^{\frac{1}{2}}(u) \right], \\ \phi_\pi^T(x) &= \frac{f_\pi}{2\sqrt{6}} (1 - 2x) \left[ 1 + 0.56 (1 - 10x + 10x^2) \right].\end{aligned}\quad (69)$$

One can see that the coefficients (0.43, 0.11) of  $\phi_\pi^P(x)$  in Eq.(69) are close to (0.59, 0.09) in Eq.(55), but the coefficient 0.56 of  $\phi_\pi^T(x)$  in Eq.(69) is much larger than 0.019 in Eq. (55). Because the coefficient 0.019 is too small, the twist-3 nonasymptotic  $\phi_\pi^T(x)$  as given in Eq. (55) is in fact the same one as the asymptotic  $\phi_\pi^T(x)$  as given in Eq. (54). This is a little unreasonable in our opinion.

- (iii) For the LO twist-2 contribution  $F_{\text{LO-T2}}^+(Q^2)$ , the theoretical prediction remain stable in the whole range of  $1 \leq Q^2 \leq 100 \text{ GeV}^2$  when asymptotic  $\phi^A(x)$  is used. While it becomes a little bit large along with the increase of  $Q^2$  when other two sets pion DA's are employed, since the twist-2  $\phi_\pi^A(x)$  in Eqs.(55,56) are very similar with each other.
- (iv) For the NLO twist-2 contribution, the value of  $Q^2 F_{\text{NLO-T2}}^+(Q^2)$  becomes smaller rapidly in the low- $Q^2$  region, say  $1 \leq Q^2 \leq 3 \text{ GeV}^2$ , and then decrease slowly from  $\sim 0.044$  to  $0.030$  along with the increase of  $Q^2$  from 3 to  $100 \text{ GeV}^2$ . The ratio  $R_1$  is changing from  $\sim 60\%$  for  $Q^2 = 3 \text{ GeV}^2$  to  $\sim 26\%$  for  $Q^2 = 100 \text{ GeV}^2$ .
- (v) For the LO twist-3 contribution, the theoretical predictions for  $Q^2 F_{\text{LO-T3}}^+(Q^2)$  obtained by using the Set-C pion DA's are about 15% larger than those obtained when the asymptotic  $\phi_\pi^{P,T}$  are used, but much smaller than the ones from the Set-B pion DA's. The reason is of course the special choice of  $\phi_\pi^T(x)$  in Set-B pion DA's. In the low- $Q^2$  region of  $Q^2 < 10 \text{ GeV}^2$ , the LO twist-3 contribution becomes small rapidly. From the numbers in Table I for the case of Set-C pion DA's, one can see that the ratio between the LO twist-3 and LO twist-2 contribution are approximately 7.3, 1.6, 0.9 for  $Q^2 = 1, 5, 10 \text{ GeV}^2$  respectively. This is rather different from the behavior when Set-B pion DA's are used, in which the LO twist-3 part is always larger than the LO twist-2 contribution by a factor  $\geq 4.1$ .
- (vi) For the NLO twist-3 contribution, the theoretical predictions for  $Q^2 F_{\text{NLO-T3}}^+(Q^2)$  has an opposite sign with its counterpart  $Q^2 F_{\text{NLO-T2}}^+(Q^2)$  and largely canceled each other. The

NLO twist-3 contribution calculated by using the Set-A and Set-C pion DA's are similar in size ( the difference is around 10% ) in the whole range of  $Q^2$  and become smaller rapidly along with the increase of  $Q^2$ , as illustrated by the lowest dot-dash curves in Figs.7 and 9. The  $Q^2 F_{\text{NLO-T3}}^+(Q^2)$  from the Set-B pion DA's is similar in size with those for other two cases at the starting point  $Q^2 = 1 \text{ GeV}^2$ , but remain basically stable in the range of  $Q^2 > 3 \text{ GeV}^2$ .

- (vii) The ratio  $R_1$  from the three different sets of pion DA's has similar value and  $Q^2$ -dependence, as illustrated by the upper dots curves in Fig. 10. The other three ratios  $R_{2,3,4}$  as shown in Fig. 10(a) and 10(c) are also similar in size and in their  $Q^2$ -dependence, but rather different from those obtained by using the Set-B pion DA's. The ratio  $R_2$  in Fig. 10(c), for example, is changing from  $-0.552$  for  $Q^2 = 1 \text{ GeV}^2$  to  $-0.199$  for  $Q^2 = 100 \text{ GeV}^2$ , while the ratio  $R_2$  in Fig. 10(b) changes its value from  $-0.288$  for  $Q^2 = 1 \text{ GeV}^2$  to  $-0.503$  for  $Q^2 = 100 \text{ GeV}^2$ .
- (viii) When the Set-C pion DA's are used, one can see from the Table II and Fig. 10(c) that (a) at twist-2 level, the NLO twist-2 contribution can provide a strong enhancement to the LO twist-2 part, from 30% to 60% in the range of  $3 < Q^2 \leq 100 \text{ GeV}^2$ ; (b) at twist-3 level, the NLO twist-3 contribution is about 30% of the LO twist-3 part in magnitude in the range of  $3 < Q^2 \leq 10 \text{ GeV}^2$ , but has an opposite sign with its LO counterpart in the whole range of  $Q^2$ , which leads to a partial cancelation of the LO and NLO twist-3 contributions;
- (ix) Because of the strong cancelation between the NLO twist-2 and NLO twist-3 contributions, the total NLO contribution to pion form factor  $F^+(Q^2)$  become small in size with respect to the total LO part, from about  $-31\%$  for  $Q^2 = 1 \text{ GeV}^2$  to  $\sim 25\%$  for  $Q^2 = 100 \text{ GeV}^2$  when the Set-C pion DA's are used. The ratio  $R_3$  change its sign at the point  $Q^2 \sim 6 \text{ GeV}^2$ , as shown by the solid curve in Fig. 10(c). When the Set-B pion DA's are used, however, the ratio  $R_3$  is always negative and keep stable in size for the whole range of  $Q^2$ .

## V. CONCLUSION

In this paper, we made the first calculation for the NLO twist-3 contributions to the pion electromagnetic form factor for the  $\pi\gamma^* \rightarrow \pi$  process, by employing the  $k_T$  factorization theorem and using the nonasymptotic pion distribution amplitudes: the leading twist-2  $\phi_\pi^A(x)$  the twist-3  $\phi_\pi^{P,T}(x)$ .

The UV divergences at the NLO twist-3 level are found to be the same ones as the NLO twist-2 part, which confirms the universality of the non-perturbative wave functions. These UV divergences are renormalized into the coupling constants and quark fields. Both the soft and collinear divergences in the NLO QCD quark diagrams and in the NLO effective diagrams for pion wave functions are regulated by the off-shell momentum  $k_T^2$  of the light quark. The soft divergences cancels themselves in the quark diagrams and the collinear divergences cancels between the QCD quark diagrams and the effective diagrams at twist-3, in cooperation with the cancelation at the leading twist-2 [9], verified the validity of the  $k_T$  factorization for the exclusive decays at the NLO level. The large double logarithm  $\ln^2 x_i$  in the NLO hard kernel are strongly suppressed by the Sudakov factor, then the NLO corrections are under control.

From the analytical calculations we obtained two factors  $F_{\text{T3}}^{(1)}(x_i, t, Q^2)$  and  $\bar{F}_{\text{T3}}^{(1)}(x_i, t, Q^2)$ , which describe directly the NLO twist-3 contributions to the pion form factors  $F^+(Q^2)$  as shown

in Eq. (63). From the numerical results and phenomenological analysis we found the following points:

- (i) For the LO twist-2, twist-3 and NLO twist-2 contributions, our results agree very well with those as given in previous work [9] for both the magnitude and the  $Q^2$ -dependence of the individual part.
- (ii) The newly calculated NLO twist-3 contribution is negative in sign and will interfere destructively with the NLO twist-2 part, leaves a relatively small total NLO contribution, which can result in a roughly  $\pm 20\%$  corrections to the total LO contribution in almost all considered ranges of  $Q^2$ .
- (iii) The theoretical predictions for  $Q^2 F^+(Q^2)$  in the low- $Q^2$  region agree well with currently available data. The inclusion of NLO contributions results in a better agreement between the theory and the experiments.
- (x) The theoretical predictions for the pion form factors obtained by employing the  $k_T$  factorization theorem have a moderator dependence on the form and the shape of the pion distribution amplitudes, this is the main source of the theoretical uncertainty.

## VI. ACKNOWLEDEMENT

The authors would like to thank Hsiang-nan Li, Cai-Dian Lu, Xin Yu, Yu-Ming Wang and Yue-Long Shen for collaborations and valuable discussions. This work is supported by the National Natural Science Foundation of China under Grant No.10975074,11235005, and by the Project on Graduate Students Education and Innovation of Jiangsu Province under Grant No. CXZZ13-0391.

- 
- [1] J. Botts and G. Sterman, **Nucl. Phys. B** **325**, 62 (1989); H.N. Li and G. Sterman, **Nucl. Phys. B** **381**, 129 (1992); T. Huang and Q.X. Shen, **Z. Phys. C** **50**, 139 (1991); F.G. Cao, T. Huang and C.W. Luo, **Phys. Rev. D** **53**, 5358(1995).
  - [2] J.C. Collins and R.K. Ellis, **Nucl. Phys. B** **360**, 3 (1991).
  - [3] H.N. Li and H.L. Yu, **Phys. Rev. Lett.** **74**, 4388 (1995); **Phys. Lett. B** **353**, 301 (1995); **Phys. Rev. D** **53**, 2480 (1996).
  - [4] Y.Y. Keum, H.N. Li and A.I.Sanda, **Phys. Lett. B** **504**, 6 (2001), **Phys. Rev. D** **63**, 054008 (2001).
  - [5] C.D. Lü, K. Ukai and M.Z. Yang, **Phys. Rev. D** **63**, 074009 (2001).
  - [6] S. Catani, M. Ciafaloni and F. Hautmann, **Phys. Lett. B** **242**, 97 (1990), **Nucl. Phys. B** **366**, 135 (1991).
  - [7] J.P. Ralston and B. Pire, **Phys. Rev. Lett.** **65**, 2343 (1990).
  - [8] S.Nandi and H.N. Li, **Phys. Rev. D** **76**, 034008 (2007).
  - [9] H.N. Li, Y.L. Shen, Y.M. Wang and H.Zou, **Phys. Rev. D** **83**, 054029(2011).
  - [10] H.N. Li, Y.L. Shen, Y.M. Wang, **Phys. Rev. D** **85**, 074004 (2012).
  - [11] H.N. Li, **Phys. Rev. D** **64**, 014019(2001).
  - [12] T. Kurimoto, H.N. Li, and A.I. Sanda, **Phys. Rev. D** **65**, 014007 (2001).
  - [13] C.D. Lü and M.Z. Yang, **Eur. Phys. J. C** **23**, 275-287 (2002).
  - [14] H.N. Li, **Phys. Rev. D** **66**, 094010 (2002).

- [15] H.N. Li, **Phys. Lett. B** **555**, 197 (2003).
- [16] B.W.Harris and J.F.Owens, **Phys. Rev. D** **65**, 094032 (2002).
- [17] V.M. Braun and I.E. Filyanov, **Z. Phys. C** **48**, 239 (1990).
- [18] P. Ball, **J. High Energy Phys.** **9901**, 010 (1999).
- [19] P. Ball, V.M.Braun and A.Lenz, **J. High Energy Phys.** **0605**, 004 (2006), P. Ball, V.M. Braun, Y. Koike, and K. Tanaka, **Nucl. Phys. B** **529**, 323 (1998), P. Ball, **J. High Energy Phys.** **9809** (1998) 005.
- [20] Y.U. Chun and H.N. Li, **Phys. Rev. D** **84**, 034018 (2011).
- [21] W. Siegel, **Phys. Lett. B** **84**, 193 (1979).
- [22] M. Nagashima and H.N. Li, **Eur. Phys. J. C** **40**, 395 (2005).
- [23] J.P. Ma and Q. Wang, **J. High Energy Phys.** **0601**, 067 (2006); **Phys. Lett. B** **642**, 232 (2006).
- [24] X.Ji and F.Yuan, **Phys. Lett. B** **543**, 66 (2002).
- [25] J.C. Collins, **Acta. Phys. Polon. B** **34**, 3103 (2003).
- [26] H.N. Li, [arXiv:1308.0413](https://arxiv.org/abs/1308.0413).
- [27] H.N. Li, Y.L. Shen and Y.M. Wang, **J. High Energy Phys.** **1302**, 008 (2013).
- [28] H.N. Li, Y.L. Shen and Y.M. Wang, [arXiv:1310.3672](https://arxiv.org/abs/1310.3672).
- [29] M. Nagashima and H.N. Li, **Phys. Rev. D** **67**, 034001 (2003).
- [30] P. Ball and R. Zwicky, **Phys. Rev. D** **71**, 014015 (2005).
- [31] H.N. Li, S. Mishima, and A. I. Sanda, **Phys. Rev. D** **72**, 114005 (2005).
- [32] H.S. Wang, X. Liu, Z.J. Xiao, L.B. Guo, and C.D. Lü, **Nucl. Phys. B** **738**, 243 (2006); Z.J. Xiao, Z.Q. Zhang, X. Liu, and L.B. Guo, **Phys. Rev. D** **78**, 114001 (2008).
- [33] Z.J. Xiao, W.F. Wang, and Y.Y. Fan, **Phys. Rev. D** **85**, 094003 (2012); W.F. Wang and Z.J. Xiao, **Phys. Rev. D** **86**, 114025 (2012); Y.Y. Fan, W.F. Wang, S. Cheng, and Z.J. Xiao, **Phys. Rev. D** **87**, 094003 (2013).
- [34] Z.T. Wei and M.Z. Yang, **Phys. Rev. D** **67**, 094013 (2003).
- [35] H.N. Li and B. Tseng, **Phys. Rev. D** **57**, 443 (1998).
- [36] C.J.Bebek et al, **Phys. Rev. D** **17**, 1693 (1978).
- [37] G.M.Huber et al, (Jefferson Lab Collaboration), **Phys. Rev. C** **78**, 045203 (2008).